

UNIVERSITÉ DU QUÉBEC À MONTRÉAL

NEOTECTONIC SUBSIDENCE, SEDIMENT TRANSPORT, LITHOSPHERIC  
FLEXURE AND MANTLE CONVECTION ABOUT FOUR MAJOR FLUVIAL  
BASINS: A DYNAMICAL LINK

DISSERTATION  
PRESENTÉD  
AS PARTIAL REQUIREMENT  
FOR MASTER'S DEGREE IN EARTH SCIENCES

BY  
PAUL AUERBACH

APRIL 2011

UNIVERSITÉ DU QUÉBEC À MONTRÉAL  
Service des bibliothèques

Avertissement

La diffusion de ce mémoire se fait dans le respect des droits de son auteur, qui a signé le formulaire *Autorisation de reproduire et de diffuser un travail de recherche de cycles supérieurs* (SDU-522 – Rév.01-2006). Cette autorisation stipule que «conformément à l'article 11 du Règlement no 8 des études de cycles supérieurs, [l'auteur] concède à l'Université du Québec à Montréal une licence non exclusive d'utilisation et de publication de la totalité ou d'une partie importante de [son] travail de recherche pour des fins pédagogiques et non commerciales. Plus précisément, [l'auteur] autorise l'Université du Québec à Montréal à reproduire, diffuser, prêter, distribuer ou vendre des copies de [son] travail de recherche à des fins non commerciales sur quelque support que ce soit, y compris l'Internet. Cette licence et cette autorisation n'entraînent pas une renonciation de [la] part [de l'auteur] à [ses] droits moraux ni à [ses] droits de propriété intellectuelle. Sauf entente contraire, [l'auteur] conserve la liberté de diffuser et de commercialiser ou non ce travail dont [il] possède un exemplaire.»

UNIVERSITÉ DU QUÉBEC À MONTRÉAL

LA SUBSIDENCE NÉOTECTONIQUE, LE TRANSPORT DES SÉDIMENTS, LA  
FLEXURE LITHOSPHERIQUE ET LA CONVECTION MANTELLIQUE SUR  
QUATRE GRANDS BASSINS FLUVIAUX: UN LIEN DYNAMIQUE

MÉMOIRE  
PRÉSENTÉ  
COMME EXIGENCE PARTIELLE  
DE LA MAÎTRISE EN SCIENCES DE LA TERRE

PAR  
PAUL AUERBACH

AVRIL 2011

## ACKNOWLEDGMENTS

There is much more to this thesis than what is actually enclosed herein. The following expose is like a parked car. It cannot truly do justice to the people and labor that went into its construction. Neither, the product offers little information as to its future residence. The following short note is a humble attempt to describe the human side of this so-called stationary car.

The love and support offered unconditionally by my family and friends cannot be overstated. I owe them more than a lifetime of gratitude.

Like many successful journeys, the work accomplished is more from the input and guidance from a selection of very talented people. In my eyes, Dr. Forte, Dr. Perry, Rob Moucha and Petar Glisovic came to form an array of mentors who displayed nothing but enthusiasm for my unconventional ideas. They displayed, with encouragement, excessive patience for my wobbly learning-curve and openness to many 'out-there' ideas.

For my whole life I have become accustomed to having support from those stronger than me. Individual and collective care for my growth and wellness is the name of my game. This fortune was perpetuated as I entered GEOTOP's Geodynamics/Geophysics research team. Though it is ultimately up to me to look and learn, the giants' shoulders of whom I stand upon is soft to the touch, sturdy, and grand in stature. Much more thanks and gratitude is owed, though, to the sheltering nature and confidence inherent to this scaffold of peers. I trust these personal relationships will continue to invoke both intellectual and spiritual progress.

## ABSTRACT

Vertical subsidence associated with major active continental drainage systems is often treated separately amid the domains of geomorphology and geophysics. We presently explore the relationship between mantle dynamics and active fluvial systems. Using existing data sets and compilations, particularly the global crustal model CRUST2.0, a simple multi-step approach is undertaken to quantify what we term anomalous neotectonic subsidence (ANTS'). We use previously established methods to evaluate continent-scale isostatic crustal configuration as well as corrections to sediment loading and catchment-wide denudation. Additional parameters are introduced to the above corrections and include (1) the flexural response to sedimentary flux and offshore deltaic loading and (2) a large-scale crustal restoration unique to this study. Focusing our study on some of the largest active terrestrial basins and their oceanbound major arterial rivers, a pattern of systematic anomalous negative positioning (ANTS') emerges. Pliocene-Recent geomorphological and neotectonic history of each region is taken into account in the effort to understand the near-surface expression of marked subsidence values. Signals of ANTS' for selected basins are additionally considered with respect to geophysical observables and global geodynamic model predictions. Through two rather novel approaches to simple basin-scale fluvial modeling, we establish a first-order connection between basin scale near-surface features and deep-earth processes. In this way, geologically recent sediment routing systems are contextualized within a geodynamic framework: The connections proposed in this study suggest the evaluation of both geological processes and the evolving earth should be regarded as a finely balanced integrated system with complex feedbacks between the surface and the deep interior.

Keywords: basin subsidence, isostasy, dynamic topography, flexural rebound, sediment routing, fluvial

## RÉSUMÉ

La subsidence verticale associée aux majeurs systèmes de drainage continentaux actifs est souvent étudiée en dehors de toute considération géomorphologique et géophysique. Nous allons explorer les relations entre la dynamique mantellique et les systèmes fluviaux actifs. En utilisant les bases de données et les compilations existantes, notamment le modèle crustal global CRUST 2.0, nous quantifierons grâce à une approche simple par itérations ce qui est communément appelé la subsidence néotectonique anormale (ANTS'). Nous utiliserons des méthodes existantes pour évaluer la configuration crustale isostatique à l'échelle du continent et aussi les corrections à appliquer à la surcharge sédimentaire et à la dénudation à l'échelle du bassin versant. Des paramètres additionnels seront introduits aux corrections précédentes et inclus à (1) la réponse flexurale au flux sédimentaire et à la surcharge sédimentaire au niveau des deltas offshore et (2) la restauration crustale à grande échelle. La focalisation de notre étude sur des bassins continentaux actifs parmi les plus importants à la surface de la terre et sur des fleuves majeurs met en exergue un pattern d'anomalie négative systématique (ANTS'). L'histoire géomorphologique et néotectonique Pliocène à aujourd'hui de chaque région sera prise en compte dans nos efforts visant à comprendre l'expression de sub-surface des valeurs de subsidence observées. Les signaux de L'ANTS' pour les bassins sélectionnés seront de plus considérés du point de vue des observables géophysiques et de prédictions des modèles géodynamiques. A travers la mise en application de deux nouvelles approches de la modélisation simple de l'hydrologie à l'échelle d'un bassin, nous établirons une connexion de premier ordre entre les caractéristiques de sub-surface à l'échelle du bassin et les processus des enveloppes profondes. Nous intégrerons donc les systèmes classiques d'étude des sédiments récent dans une approche géodynamique contextuelle : Les relations proposées dans cette étude suggèrent que l'évaluation à la fois des processus géologiques et de l'évolution du système Terre doit être approchée en intégrant finement les relations entre les processus de surface et les processus internes.

Mots clés: subsidence vertical, réponse flexurale, dynamique mantellique, l'hydrologie, bassin

## TABLE OF CONTENTS

INTRODUCTION.....	1
CHAPTER 2	
DATA SOURCES.....	3
2.1 Global Topography.....	3
2.1.1 Crustal Structure.....	3
2.1.2 Description.....	3
2.1.3 Previous Usage.....	4
2.1.4 Supplementary Crustal Data.....	5
2.2 Physiographic Data.....	6
2.2.1 Major Rivers.....	6
2.2.2 River Catchment Areas and Drainage Divides.....	6
2.2.3 Basin Surface Lithologies.....	7
2.3 Denudation Rates.....	8
2.4 Faults.....	8
2.5 Gravity.....	8
2.6 Dynamic Topography and Mantle Structure.....	9
CHAPTER 3	
METHODOLOGY AND PARAMETERS.....	12
3.1 Isostasy.....	12
3.1.1 CRUST2.0 Isostatic Crustal Configuration.....	12
3.1.2 Residual Topography.....	14
3.2 Flexural Isostasy.....	14
3.2.1 Flexural Properties.....	16
3.2.2 Basin Flexure.....	16
3.3 Mechanisms of Subsidence.....	19
3.4 Treatment of Anomalous Subsidence.....	20
3.4.1 Subsidence due to Sediment Loading.....	20
3.4.2 Subsidence due to Crustal Effects.....	21
3.5 Anomalous Neo-Tectonic Subsidence.....	22
3.5.1 Basins with ANTS in Space and Time.....	22
CHAPTER 4	
RESULTS.....	24
4.1 Isostatic Topography.....	24
4.1.2 Residual Isostatic Topography.....	24
4.2 Isostatic Restoration of Sedimentary Loads.....	25
4.2.1 Crustal Restoration Level.....	26

4.3 Anomalous Neotectonic Subsidence.....	27
4.4 Flexural Response to Erosion and Deposition.....	28
4.4.1 Input Parameters.....	29
4.4.2 Flexural Model Results.....	30
4.5 Denudational Isostatic Uplift.....	37
4.6 Corrected Anomalous Neo-Tectonic Subsidence (ANTS').....	38
 CHAPTER 5	
DISCUSSION.....	41
5.1 Physiography of Nile River Basin.....	41
5.1.1 Structural Features of the Nile in Northern Sudan and Egypt.....	41
5.1.2 L.Miocene to Recent Egyptian Nile Basin Sedimentary Dynamics...42	
5.2 Physiography of the Amazon River Basin.....	42
5.2.1 Regional Structure.....	43
5.2.2 L.Miocene to Recent Sed. Dynamics of the Amazon River.....	43
5.3 Physiography of the Mississippi Embayment.....	45
5.3.1 Regional Structure.....	46
5.3.2 Pliocene to Recent Sed. Dynamics of the Lower Miss. River.....	46
5.4 Physiography of the Niger River Basin.....	47
5.4.1 Regional Structure.....	47
5.4.2 L. Miocene to Recent Sed. Dynamics of the Lower Niger Basin.....	48
5.5 Geophysical Observables.....	48
5.6 Reconstructed Mantle Temperature Anomalies.....	51
 CHAPTER 6	
CONCLUSIONS.....	56
6.1 Motivation.....	56
6.2 Importance of Crustal Structure.....	56
6.3 Isostatic and Flexural Assumption.....	57
6.4 Simplified Fluvial Modeling.....	58
6.5 Time-Dependent Rheology.....	59
6.6 Concluding Comments and Remarks.....	60
 REFERENCES.....	61
 Appendix 1 .....	73
Appendix 2 .....	75

## List of Figures

Figure 1.1 Dynamic Topography For the Studied Fluvial Basins.....	2
Figure 2.1 Global map of modern-day drainage basins and catchment divide.....	8
Figure 2.2 Dynamic Surface Topography derived from joint seismic-geodynamic tomography model.....	11
Figure 3.1 Schematic representations of crustal columns configured in CRUST2.0.....	13
Figure 3.2 Schematic illustration of Airy-isostatic and flexural isostatic responses.....	19
Figure 4.1 Isostatic and Non-Isostatic Topography based on structure of CRUST2.0.....	25
Figure 4.2 Sediment-loading and crustal restoration corrections for continents.....	26
Figure 4.3 Anomalous neo-tectonic subsidence (ANTS) for intrabasinal areas.....	28
Figure 4.4 ETOPO2 DEM with selected river segments used in flexural modeling.....	29
Figure 4.5 Imposed anti-loads and loads distributed across river transects.....	32
Figure 4.6 Corrected Anomalous neo-tectonic subsidence corrected (ANTS').....	39
Figure 5.1 Physiographic map compilations of four active fluvial basins.....	44
Figure 5.2 Crust-corrected free-air surface gravity anomalies for selected basins.....	50
Figure 5.3 Radial cross-sections of reconstructed mantle temperature variations.....	52
Figure A.1 Schematic cross sections of imposed sedimentary loading/unloading.....	73
Figure A.2 Map view of transect paths on true earth topography and prescribed loads....	75

## List of Symbols and Abbreviations

Force	(N, Newtons)
Mass	(M, Kilograms)
Length	(L, Meters or Kilometers)
Area	(L <sup>2</sup> )
Volume	(L <sup>3</sup> )
Anomalous Neotectonic Subsidence	(ANTS, L)
Corrected Anomalous Neotectonic Subsidence	(ANTS', L)
Isostatic Topography	(H <sub>iso</sub> , L)
Residual Topography	(H <sub>res</sub> , L)
Observed Topography	(H <sub>obs</sub> , L)
Lithospheric Elastic Thickness	(T <sub>e</sub> , L)
Height of Sedimentary Load	(h, L)
Effective Rigidity	(D, NL)
Flexural Parameter	(α, 1/L)
Inverse Flexural Parameter	(φ, L)
Density of Sediments	(s, M/V)
Density of Crust	(ρ <sub>c</sub> , M/V)
Density of Mantle	(ρ <sub>m</sub> , M/V)
Bulk Modulus	(E, GPa)
Poisson's Ratio	(ν, dimensionless)
Vertical Isostatic Loading Response	(ISC, L)
Thickness of Sediments	(t, L)

Height of Flexural Deflection	( $W, L$ )
Horizontal Coordinate	( $x, L$ )
Half-width of Sedimentary Load	( $s, L$ )
Distance of Load from Origin	( $X, L$ )
Crustal Layer Thickness	( $c, L$ )
Crustal Layer Density	( $\rho, M/V$ )
Height of Isostatic Deflection	( $\delta c, L$ )
Crustal Isostatic Correction	( $H'_{iso}, L$ )
Vertical Flexural Correction	( $\omega_l, L$ )
Vertical Isostatic Response to Denudation	( $D_{rdb}, L$ )
Downward Force	(N/A)
Horizontal Force	(N/A)

## Introduction

Subsidence is perhaps one of the most prominent geodynamic phenomenon related to the evolution of terrestrial basins. Many studies have considered anomalous, dynamically-driven subsidence over geologically long time-scales (Mitrovica et al. 1989; Gurnis 1990; Burgess and Gurnis 1995; Pysklywec and Mitrovica 1999; Pysklywec and Mitrovica 2000; Burgess and Moresi 2001; Daradich et al. 2001; Heller et al. 2003; Liu and Nummedal 2004; Spajocevic et al. 2008; Heine et al. 2008). From the presence and architecture of ancient sedimentary sequences, these studies have proven fruitful in retrodicting past geodynamics. Surprisingly, little attention has been paid to the possibility for subsidence of contemporary basins within a geodynamic framework (Hartley and Allen 1994; Wheeler and White 2002; Downey and Gurnis 2009; Crosby et al. 2010). Only recently has the geomorphology and neotectonic community addressed the role of mantle dynamics in observations of present, and geologically young, landscape features. Though promising, much of the work to date has focused on either regions associated with mantle upwelling at plate boundaries (Daradich et al. 2003; Furlong et al. 2006; Faccenna et al. 2007) or, similarly, landscape response to positive dynamic topography (Furlong et al. 2006; Lock et al. 2007; D'Agostini et al. 2008).

The current study is initiated by the observation where both the dynamic topography generated from 3-D mantle convection simulations and the non-isostatic topography fields from CRUST2.0, alike, show systematic negative amplitudes about major active fluvial basins. Naturally, we are inclined to explore this intriguing correlation and seek to resolve the underlying dynamical basis of this connection by studying current representations of internal mantle structure. Under the assumption that mantle convection is ultimately driven by buoyancy forces arising from thermal ( and chemical) density contrasts, we conclude the following study with supplementing evaluations of (1) a crust-corrected global free-air gravity model and (2) reconstructed, whole-mantle temperature fields under the regions pertinent to this study.

Based on the apparent success of past studies in establishing the significance of mantle dynamics with respect to near-surface processes, we feel it timely to address present-day basins from a similar vantage point. This is especially salient since present-day dynamic topography

(Fig. 1.1) can be regarded with relative confidence. Since the spatial and temporal scales of basins (*e.g.* Potter 1978; Miall 2007) are comparable to the characteristic wavelengths and general rates of dynamic topography changes (Moucha et al. 2008; Heine et al. 2008), their mutual-inclusion seems quite fitting.

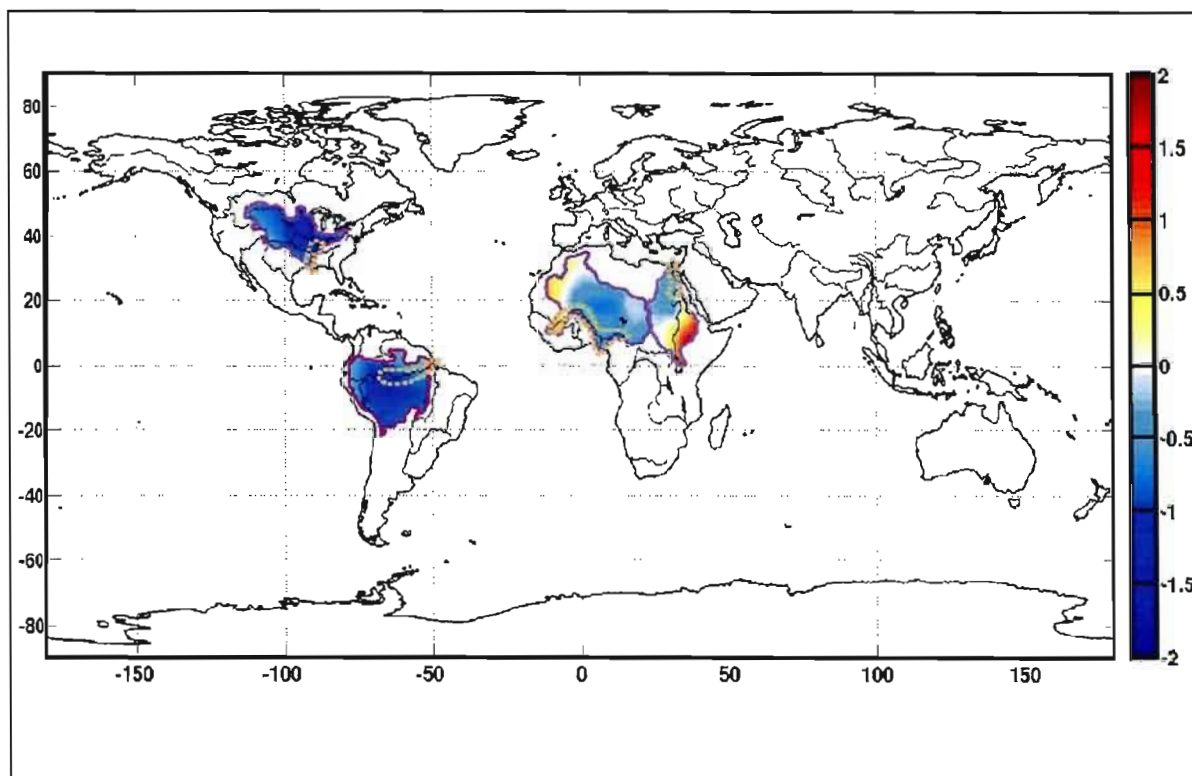


Figure 1.1 Present-day dynamic surface topography (kilometers) derived from joint seismic-geodynamic tomography model (Simmons et al. 2007) for studied river basins. Yellow dotted outlines mark both main trunk rivers of the selected basins as well as the spatial extent of the 2-D isostatic flexural modeling performed in this study (see results displayed in Chapter 4). Note the general pattern of negative surface dynamic topography associated with the lower portions (marginal to shore proximal) of each basin's respective river system.

## 2. Data Sources

### 2.1 Global Topography:

In this study we utilize the ETOPO2v2 database (NGDA 2006) for the relief of the earth's surface. The gridded data has a 2' horizontal resolution, corresponding to approximately 4 km at the equator, and a vertical precision of 1m. The horizontal and vertical datum is the reference ellipsoid of WGS-84 and mean-sea level, respectively. Although databases of greater resolution are available (e.g. SRTM, GTOPO30), ETOPO2v2 is sufficient for regional to continental scale analysis. Furthermore, it is both seamless and formatted for computational analysis.

### 2.1 Crustal Structure:

The global CRUST2.0 (Laske (2004), Laske and Masters (1997)) data set is used to capture broad scale crustal thickness and density variations over the continents. Primarily, the structure is employed in this study to constrain continental isostatic and residual topography fields. The 1°x 1° sediment thickness compilation (Laske and Masters 1997) is employed for several intraplate basin analyses.

### 2.1.2 Description:

The CRUST2.0 global crustal model, resolved at  $2^\circ \times 2^\circ$ , emanated from an earlier  $5^\circ \times 5^\circ$  global compilation of crustal structure (Mooney et al. (1998)). We herein concentrate on the most recent CRUST2.0 model (Laske (2004)) with reappraised sediment layers at a resolution of  $1^\circ \times 1^\circ$ .

Each  $2^\circ \times 2^\circ$  cell is ascribed to one of 360 geologic settings, based on a nominal form of Epoch (e.g. Phanerozoic, Mesozoic), tectonic setting and occasional qualifier (e.g. melt-affected rift, island arc, pull-apart basin), geologic/physiographic state (e.g. continental margin, platform, craton), and sediment thickness (e.g. no sediment, 1km sediment, etc.). The descriptions are generalized and represented in Plate 1a of Mooney et al. (1998).

The model structure is based on seismic data that include compressional wave velocities ( $V_p$ ), shear wave velocities ( $V_s$ ) and two-way travel times (TWT). From these measurements the model is vertically stratified into 7 layers, where the top two layers are water and ice. Five layers comprise the crust: (1) soft sediments (layer 3), (2) hard sediments (layer 4), (3) upper crust or basement (layer 5), (4) middle crust (layer 6) and, (5) lower crust (layer 7). The base of layer 7 defines the Moho interface between the crust and underlying upper mantle. Each layer has a thickness and a density, the latter formulated from seismic-velocity to density conversions (Christensen and Mooney (1995)). The sum of layers 3-7 is taken as the crustal thickness for the given cell. The base of the crust rests on a denser layer of unspecified thickness taken to represent the mantle lithosphere.

### 2.1.3 Previous Usage

Although CRUST2.0 is a simplification of the earth's global crustal structure, it has yet to be replaced by an updated global crustal compilation. Numerous, inter-disciplinary studies have employed aspects of the model to explore a wide range of geophysical phenomena. This does not completely validate the model, but does attest to its general acceptance by numerous researchers. Table 1.1 is an overview of geophysical domains and scale by which CRUST2.0 has

been used. Obviously there are uncertainties within CRUST2.0, so we have included a section in the table that lists the main constraint, when specified, that may have affected the researchers' respective findings.

#### 2.1.4 Supplementary Crustal Data

Understandably, certain geographical regions are more constrained than others with regard to crustal structure (see Fig.1 of Mooney et al. (1998)). When assessing regional scale structure and sediment thicknesses, data from CRUST2.0 may be supplemented with site-specific data from other authors.

**Table 2.1** Previous Usages of CRUST2.0

Domain	Parameter(s)	Scale/Locale <sup>(ref)</sup>	Quantification/ Implications	Uncertainty
Thermal Isostasy/Dynamic Topography	Crustal Thickness/Densities	North America <sup>12</sup> Africa <sup>13,18</sup>	Lithospheric Chemistry/Longevity of sub-crustal Continental Roots	Accuracy of N.America and African Crustal Structure
Effective Elastic Thickness (Te)	Crustal Densities	Europe <sup>5</sup> S.America <sup>4</sup>	Gravity Anomalies, Te; Continental Longevity	Resolution of CRUST2.0
Stress Field	Crustal Thickness/Densities	Global <sup>1</sup>	Horizontal,Radial Traction/Intraplate Stress	Lower Crustal Densities and Composition
Gravitational Potential Energy (GPE)	Crustal Thickness/Densities	SouthwestU.S <sup>6</sup> Tibet <sup>7</sup>	Deviatoric Stress/Plate Driving Mechanism	Reference Column/ Lower Crustal Geometry <sup>6</sup>
Gravity	Crustal Thickness/Densities	Global <sup>8,15</sup>	Geoid, Free-air, Bouguer Anomalies/ Geodesy	Lower Crustal Thickness/ Compensation mechanisms
Seismicity	Crustal Thickness/Densities	India <sup>9</sup>	Depth of Seismic Activity/Failure Mechanisms	
Lithosphere and Mantle	Crustal Thickness/Densities/S-wave Velocities	Global <sup>11,14</sup> Africa <sup>12</sup> N.America <sup>12</sup>	Density of Cratonic roots/Compositional, Gravitational and Thermal State of Lithosphere	
Basin Analysis	Sediment Thickness/Sediment Loading	Africa <sup>12,15</sup> Global <sup>15</sup>	Basin Subsidence/Mantle Dynamics	Resolution vs. Basin size/ Possible underestimation of Sediment Thickness

References: 1. Forte and Perry (2000); 2. Perry et al. (2002); 3. Perez-Gussinye and Watts (2005); 4. Perez-Gussinye et al. (2007); 5. Lithgow-Bertelloni and Guynn (2004); 6. Flesch and Kreemer (2009); 7. Ghosh et al. (2006); 8. Tsoulis (2004); 9. Seitz and Krugel (2009); 10. Manglik et al. (2008); 11. Kaban et al. (2003); 12. Crosby et al. (2010); 13. Heine et al. (2008); 14. Pari and Peltier (2000); 15. Seber et al. (2001); 16. Wiczeorek (2006); 17. Daradich et al. (2003); 18. Forte et al. (2010)

## 2.2 Physiographic Data

Along with ETOPO2v2, geomorphologic parameters such as major river locations, basin drainage divides and surface lithologies are included. These features provide both qualitative and quantitative understanding of the present-day gross physiography of intracontinental regions. Furthermore, possible genetic links between regional geomorphology, tectonic setting, and geodynamic processes can be established.

### 2.2.1 Major Rivers

The location and course of major continental rivers are obtained from the vector data included in MATLAB® Mapping Toolbox. The paths of the world's large rivers are sufficiently resolved for depicting continent wide fluvial patterns, including regional meanders and the confluence of major tributaries. Both the river's headwaters and ocean outlets are well correlated with higher relief and epicontinental sediment accumulation, respectively. There is little difference between the courses and locations of the world's major rivers used in this study compared to the respective paths depicted in ARCGIS® and NASA's CIA World Data Bank II.

### 2.2.2 River Catchment Area and Drainage Divides

The watershed areas for studied intracontinental basins are delineated based on the model results of Graham et al. (1999) available through the National Geophysics Data Center (NDGC) web portal. The data set was derived from individual basin analysis and subsequent global representation. Parameters also include flow accumulation and local (higher-order) stream networks provided at 0.5° and 1° resolutions, making data merging relatively efficient. The perimeters and spatial extent of selected intracontinental drainage basins used herein are very similar to those delineated in other global-scale studies (Summerfield and Hulton (1994); Syvitski and Milliman (2007)) and independently constructed models (e.g. Global Runoff Data Center (Germany)).

### 2.2.3 Basin Surface Lithologies

The characteristics and near-surface distribution of lithologies in a given region plays a significant role in the pace and style of the sediment routing system (Allen and Allen (2005); Burbank and Anderson (2000); Von Blakenburg (2006)). Within a given basin the surface lithology will certainly vary in composition, cohesiveness, and layout. Faulting may juxtapose

strata of different rock types, fluvial incision can sub-aerially expose deeper substrate over relatively short distances, and slope failure progressively exfoliates parts of the terrain. Nonetheless, assessing the relative erodability between continental regions is essential in predicting where sediments accumulate.

A global basin-averaged lithology map (Fig. 2.1a), adapted and used by Syvitski and Milliman (2007) to model sediment delivery to the oceans, provides two useful parameters: (1) an appropriate nomination of general basin lithologies and (2) a simple ordinal parameterization that ranks lithologies by their relative erodability. The data included in the map is particularly suitable for the spatial scales addressed in this study.

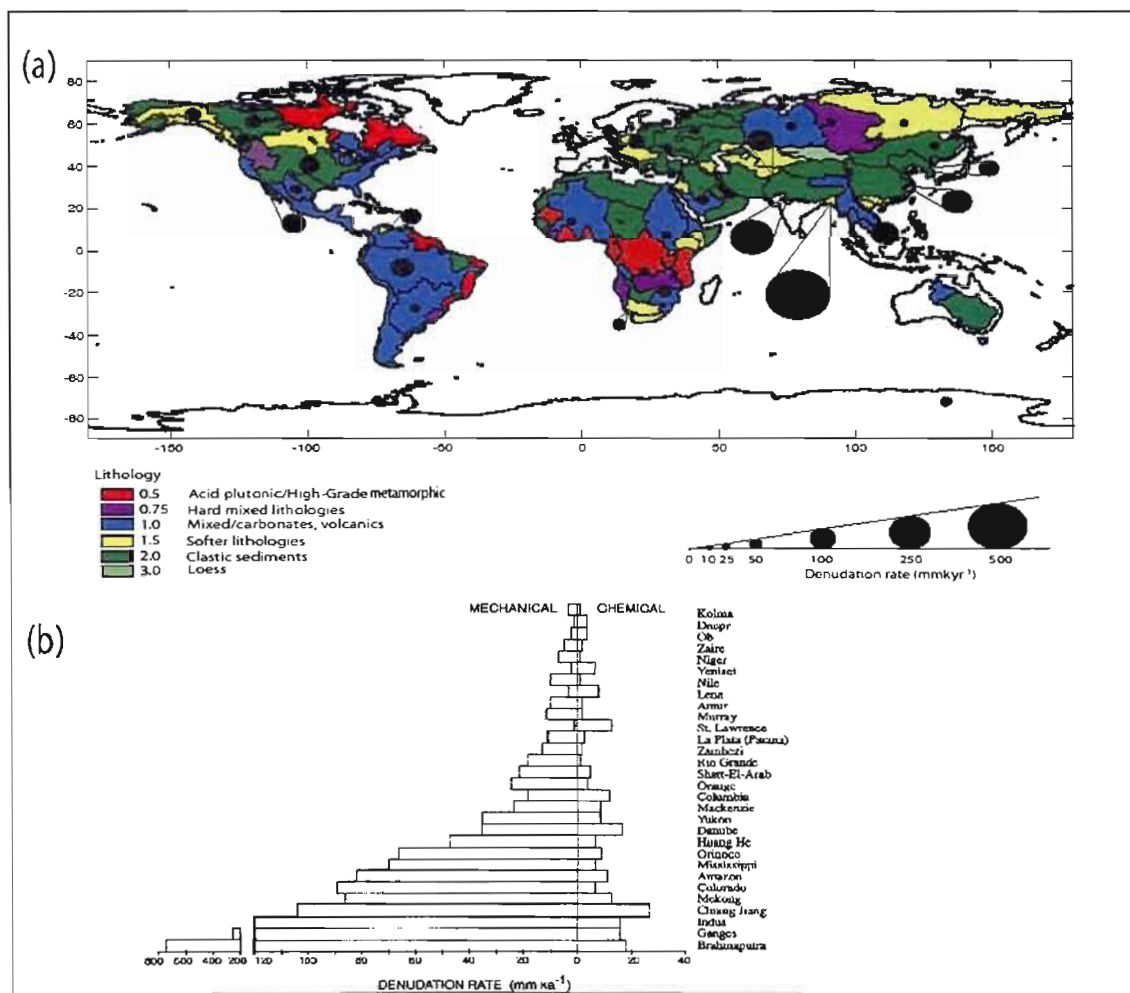


Figure 2.1 Global map of modern-day drainage basins and catchment divides (modified after Graham et al. 1999). Included are estimates of contributions by chemical and mechanical denudation rates (b) to total basin-wide denudation rates (after Summerfield and Hulton 1994) and average surface lithologies in (a). (After Syvitski and Milliman 2007).

### 2.3 Denudation Rates

The quantification of mechanical and chemical denudation is derived from sediment and solute yield (t/km<sup>2</sup>/y), respectively, divided by sediment density. Basin-wide denudation rates are general estimates that can be biased by sampling location (Allen and Allen 2005) and assumed sediment density values (Sykes (1996); Segev et al. (2006)). Many, if not all, measurements are taken at river mouths so the extent of intrabasin sediment retention and redistribution is less constrained.

For selected basins, average denudation rates (mm/kyr) are taken from the published compilations of Summerfield and Hulton (1994) and Milliman and Syvitski (1992) (Fig.2.1). Total yield measurements and basin areas can vary between datasets by 10-15%, affecting denudation estimates for particular basins. The denudation rates in Summerfield and Hulton (1994) include contribution by chemical denudation (Fig. 2.1b), effectively accounting for slightly higher estimates in their compilation. Despite some disparity, the datasets convey similar patterns and magnitudes of denudation for large externally drained continental basins.

## 2.4 Faults

Understanding the gross geomorphology of intraplate basins and their internal fluvial architecture requires the integration of fault lineaments. Fault structure, position, and orientation clarify the role of tectonic features in drainage and sediment routing. Major, long-lived rivers tend follow regional tectonic grain (Miall (2007)) and are often positioned within a fault-bounded graben or trough (e.g., Benue Trough of the Niger River and the St. Lawrence River of eastern Canada). A composite map of the world's major rift zones and their coupled fault trends are represented in Sengor and Natal'in (2001). Their maps are accompanied by a comprehensive discussion of rift geometry, age, and genesis. The compilation is ideal for the spatial scales of this study, and will serve to elucidate connections between regional architecture and surface processes. The implication that major faults may be inherently weak (Bird (1995)) and susceptible to reactivation (Ranalli (2000)) will also be addressed.

## 2.5 Gravity

Surface gravity anomalies result from variations in material density both on and beneath the earth surface. Measures of free-air gravity anomalies have been used in recent studies exploring the relationship between lithospheric structure and topography within geodynamic frameworks (Chase et al. (2009); Downey and Gurnis (2009); Crosby et al. (2010)). Current

gravity models that highlight patterns of regional and intracontinental anomalies are, to date, sufficiently constrained for basin-scale study.

Measures of free-air gravity anomalies from satellite data sets (e.g. GRACE (Tapley et al. 2005), EGM96 (Lemoine et al. 1998)) has afforded earth scientists the opportunity to further investigate regions of geologic interest (e.g. Forte 2007; Braitenberg and Ebbing 2009; Crosby and McKenzie 2009; Crosby et al. 2010; Perry and Forte 2010). Parameters such as the isostatic admittance between topography and gravity have highlighted mantle dynamical components associated with the Congo Basin (Crosby et al. 2010). Tomography-based global free-air gravity anomaly predictions, too, has increased our understanding of long-wavelength trends in the global nonhydrostatic geopotential field (e.g. Figure 15 in Forte 2007). Specific to the following study, these analyses provide additional constraints regarding the geodynamical forces operating about each basin.

## 2.6 Dynamic Topography and Mantle Structure

Inclusion of mantle structure and dynamics in assessing crustal and near-surface features provides valuable information of earth system processes. Time-dependent modeling of mantle dynamics opens up the possibility to reconstruct past geologic conditions and how the earth's outer structure has evolved to what is presently observed (Grand et al. (1997)).

Dynamic topography is a measure of the height of the earth's outer surface supported by radial stresses generated by convective flow in the mantle. The magnitude of dynamic topography, or vertical surface deflection, is the balance between vertical stresses emanating from the convecting mantle and the restoring gravitational body forces (Mitrovica et al. (1989); Lithgow-Bertelloni and Gynn (2004); Moucha et al. (2008)). The latter component is proportional to the density difference between the upper-mantle and the material overlying the earth's solid outer surface, usually taken as either air or water. Values of dynamic topography used in this study are based on 3-D mantle convection simulations incorporating a recent joint seismic-geodynamic tomography model (Simmons et al. (2009)). The current mantle convection model, and earlier versions, has been used to explain present-day stress fields (Forte et al.

(2007)), rift-flank uplift (Daradich et al. (2003); Moucha et al. (2007), Moucha et al. (2009)), as well as temporal changes in sea-level (Moucha et al. (2008)) and tectonic plate motion (Forte et al. (2009)).

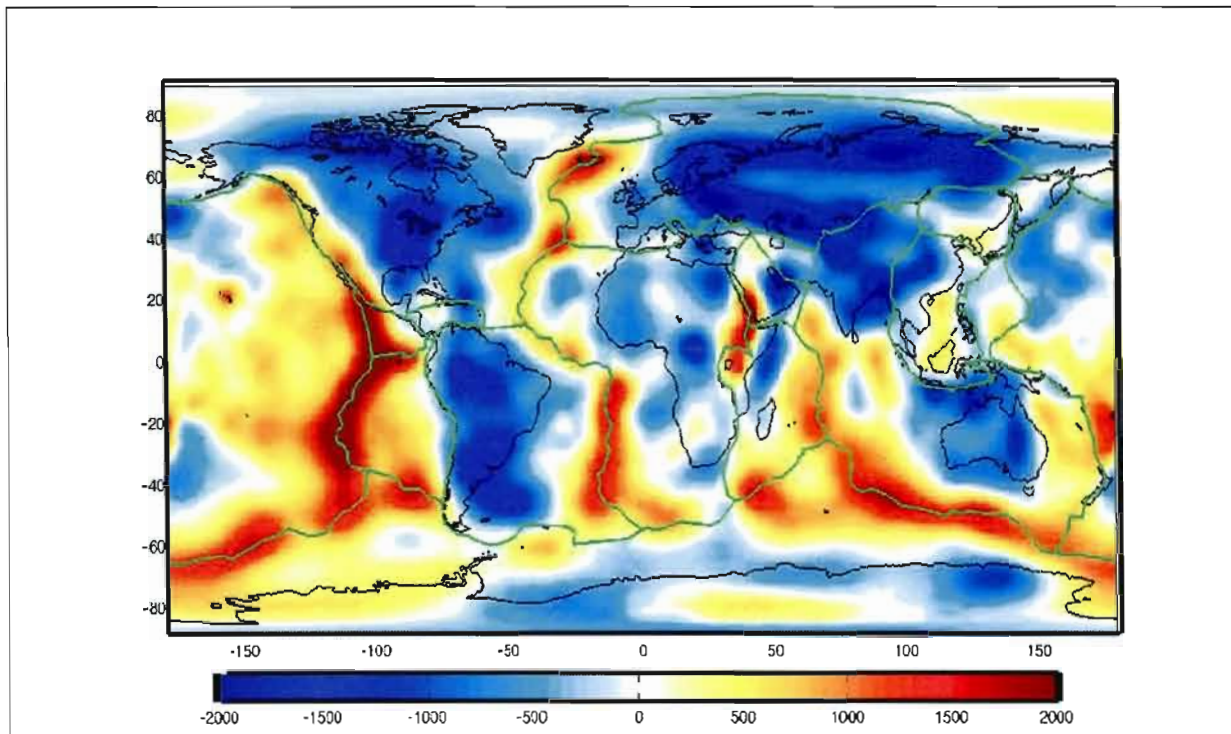


Figure 2.2 Dynamic Surface Topography (meters) derived from recent joint seismic-geodynamic tomography model (Simmons et al. 2007). Note the elevated position of spreading ridges and regions of young ocean crust and the systematic depressions associated with continental interiors and convergent margins.

### 3. Methodology and Parameters

#### 3.1 Isostasy

Isostasy implies the existence of a level surface of constant pressure within the mantle, this is called the "depth of compensation". Above this surface the mass of any vertical column is equal. Equal pressure at depth can also be achieved by varying density structure or by the regional deflection of the lithosphere. The overall configuration establishes hydrostatic equilibrium of the denser underlying medium.

##### 3.1.1 CRUST2.0 Isostatic Crustal Configuration

A simple and robust method to quantify the isostasy of CRUST2.0 is to construct an reference model of the continental crust (Pari and Peltier (2000); Perry et al. (2003)). This is obtained by averaging the thickness and density pairs  $\{c_i, \rho_i\}$  of the model layers (N) over sphere representing the earth's outer surface (Pari (2001)). The acting load of this reference column equals the support offered everywhere by the upper-mantle;

$$\sum_{i=1}^N \rho_i^{avg} c_i^{avg} = \sum_{i=1}^N \rho_i c_i + \rho_{N+1} \delta c_{(N+1)} \quad (3.1)$$

resulting in the vertical displacement of individual crustal columns (Airy-type isostasy). With respect to the background thickness configuration, solving iteratively for  $\delta c_{N+1}$  we obtain (1) the isostatic depth to the Moho, (2) the perturbation of each layer ( $\delta c_i$ ) in a local column;

$$c_i^{avg} = c_i - \delta c_{i+1} + \delta c_{(i+1)}, \rightarrow \quad i = 1, \dots, \dots, N \quad (3.2)$$

and (3) the surface deflections ( $\delta c_1$ ) (Fig 3.1). Upon subtracting the thicknesses of the water ( $c_1$ ) and ice ( $c_2$ ) layers from the magnitude of deflection for each profile, relative to the zero-elevation reference column, we solve for the isostatic topography field ( $H_{iso}$ );

$$H_{iso} = \delta c_1 - c_1 - c_2 \quad (3.3)$$

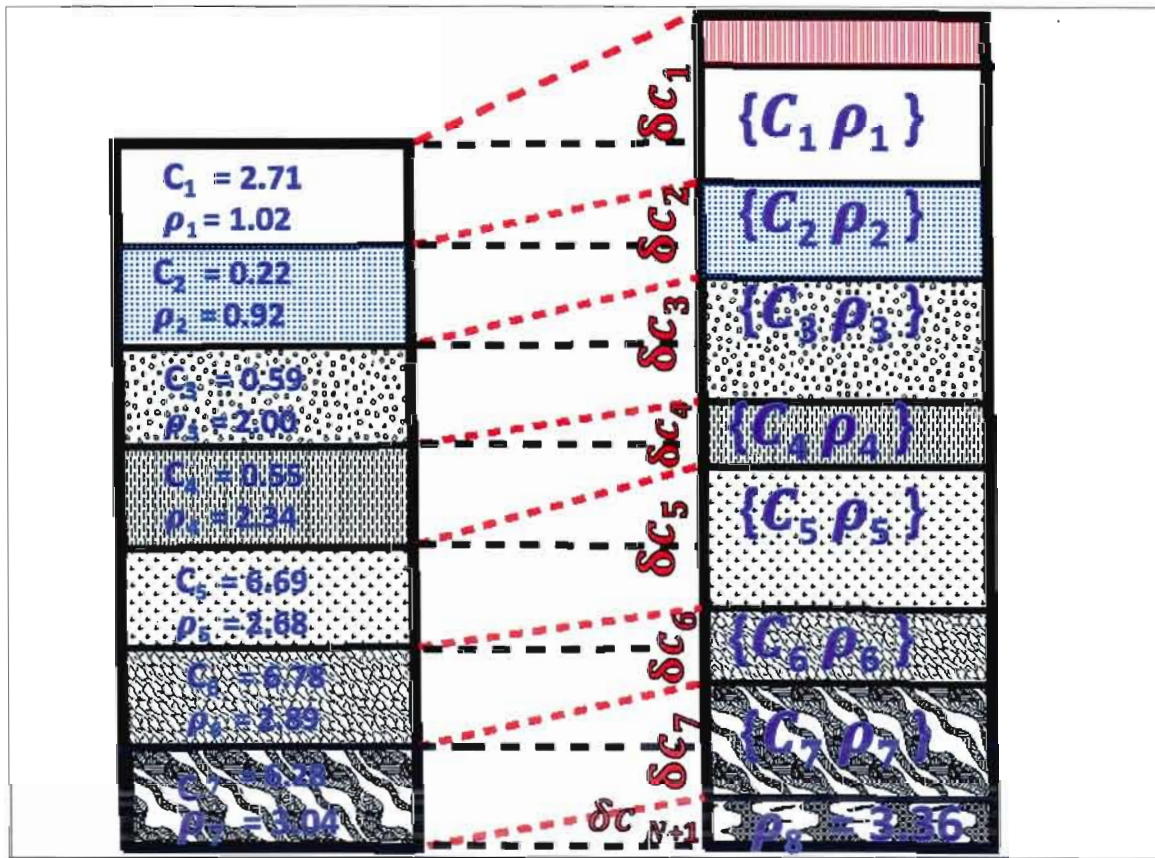


Figure 3.1. Schematic representation of two crustal columns as configured in CRUST2.0. The profile on the left represents the reference configuration derived from the mean thickness and density of each layer. The right profile is an example of a given crustal column in the model. The perturbation of each layer from the reference model (red dashed lines) is quantified by solving first for  $\delta c_{N+1}$  (see text for explanation). The isostatic surface configuration on the continents is given by  $\delta c_1$  without the water and ice layers. Not to scale. (Modified after Pari and Peltier 2000)

### 3.1.2 Residual Topography

Residual topography represents a vertical measure of how much the observed topography deviates from the elevation field produced by an isostatically balanced crust. It is constrained by subtracting the earth's true elevation field from the predicted isostatic elevations;

$$H_{residual} = H_{observed} - H_{isostatic} \quad (3.4)$$

One point to be made clear is that the isostatic elevations are a direct result of the thickness and density variations in the crustal model. The observed topography, however, represents the integrated signal of all the forces which affect its shape. Based on this reasoning, residual topography reveal the amplitudes by which earth's topography is supported by mechanisms other than the isostatic spatial distribution of crustal materials. The residual topography derived from the crustal structure of CRUST2.0 has been employed to test for the state of continental roots (Kaban et al. 2003) and the lithospheric mantle (Artemieva and Mooney 2001; Mooney and Vidale 2003) as well as to compare dynamic topography predictions emanating from mantle convection models (Forte and Perry 2000; Perry et al. 2003; Pari 2001) (see Table 1.1).

### 3.2 Flexural Isostasy

Based on the assumptions that lithospheric plates behave elastically, the flexural response to vertical loading is an overall bending of stratal interfaces. The amplitude of deflection ( $w$ ) is proportional to the strength, or effective rigidity ( $D$ ), of the lithosphere and the magnitude of external force systems given by Turcotte and Schubert (2001) as;

$$D \frac{d^4 w}{dx^4} + P \frac{d^2 w}{dx^2} + (\rho_2 - \rho_1) g w = q(x) \quad (3.5)$$

where  $q(x)$  is the downward force per unit area and  $P$  is the horizontal force. For simplicity we set  $P = 0$  and solve for the deflection based on Jordan (1981) with the parameters listed in Table 3.1.

Table 3.1 Flexural Parameters

Elastic Thickness ( $T_e$ )	20km-40km <sup>(1)</sup>
Flexural Rigidity (D)	$\frac{E \cdot T_e^3}{12(1 - \nu^2)}$
Flexural Parameters ( $\alpha, \varphi$ )	$\alpha = \left\{ \frac{4D}{\rho c g} \right\}^{1/4}$ , $\varphi = \alpha^{-1}$
Height of Load ( $h$ )	<i>Variable</i>
$\rho_1 = \text{density of sediments}$	$\rho_1 = 2000 \text{ kg/m}^3$
$\rho_2 = \text{density of mantle}$	$\rho_2 = 3300 \text{ kg/m}^3$
$\rho c = \text{density of the crust}$	$\rho c = 2750 \text{ kg/m}^3$
Material Parameters:	
Young's Bulk Modulus ( $E$ )	100 GPa <sup>(2)</sup>
Poisson's Ratio ( $\nu$ )	0.25

1. Watts (2001); 2. e.g. Jordan (1981)

### 3.2.1 Flexural Properties

Surface deflection in the context of flexural isostasy requires estimates of a plate's effective elastic thickness and mechanical properties. It is beyond the scope of this study to constrain the numerous parameters involved in quantifying lithospheric flexure; though extensive studies of rock properties, and their geologic application, underscores their importance (e.g., Turcotte and Schubert 2001; Scholz 2002; Pollard and Fletcher 2005; Christiansen and Mooney 1995). The necessary parameters, listed in Table 3.1, are derived from published estimates employed in studies of similar scale and tectonic framework.

### 3.2.2 Basin Flexure

Supracrustal loading by sediments can impart a substantial flexural response within and at the peripheries of basins (Driscoll and Karner 1994; Ussami 1999; Rodger et al. 2005; Prezzi et

al. 2009). Deflections due to surface loading and unloading can be expressed as both instantaneous (McQuarrie and Rogers 1998; Gargiani et al. 2010) or as time-dependent flexure (Blum et al. 2008; Pazzaglia and Gardner 1994). Obviously, the magnitude of flexural deformation is intimately tied to the elastic thickness ( $T_e$ ) of the lithosphere so uncertainties regarding its value will impart significant model variability.

The geometry of an unbroken elastic plate under a rectangular load is used to quantify the flexural isostatic response due to the deposition and erosion of sedimentary sequences (Fig 3.2a). The formulation by Jordan (1981), followed by Cardoza and Jordan (2001), describes the amount of deflection  $W(x)$  inboard (*ib*, to the left), directly under (*ul*), and outboard (*ob*, to the right) of a single load by;

$$W_{ib} = \frac{h \rho_1}{2 \rho_2} \left\{ \exp(-\varphi(-x + s - a)) \cos(\varphi(-x + s - a)) \right. \\ \left. - \exp[-\varphi(-x + s + a)] \cos[\varphi(-x + s + a)] \right\} \quad 3.6a$$

$$W_{ul} = -\frac{h \rho_1}{2 \rho_2} \left\{ 2 - \exp(-\varphi(x - s + a)) \cos(\varphi(x - s + a)) \right. \\ \left. - \exp[-\varphi(-x + s + a)] \cos[\varphi(-x + s + a)] \right\} \quad 3.6b$$

$$W_{ob} = \frac{h \rho_1}{2 \rho_2} \left\{ \exp(-\varphi(x - s + a)) \cos(\varphi(x - s + a)) \right. \\ \left. - \exp[-\varphi(x - s - a)] \cos[\varphi(x - s - a)] \right\} \quad 3.6c$$

where  $x$  is the horizontal coordinates (m),  $s$  is the distance of load to the center of origin (m),  $a$  is half-width of the load (m) and  $\varphi$  is the flexural parameter derived from the value of  $T_e$  (Table 3.1). The total deflection is obtained by the linear superposition of all deflections summed over the entire horizontal length. The other parameters are listed in Table 3.1.

Many of the previously noted studies have measured the total flexure over horizontal

distances less than 400km. These studies have attempted to match the amplitude of flexure with observed topography (Pazzaglia and Gardner 1994) over relatively short distances, often within convergent, thrust-related areas (e.g. Masek et al. 1994; Ussami et al. 1999).

The methodology described by Equation 3.6 is herein viewed in an alternative light. First of all, the horizontal length scales of selected basins addressed in this study are two to three times greater than previous models; i.e., the lateral extent of individual loads prescribed in this study range from 100km - 400km and the entire distance over which variably sized loads are juxtaposed reach 1000km - 1400km. This is significant because we now attempt to bridge distances relegated to either flexural responses (e.g. McQuarrie and Rogers 1998; Small and Anderson 1999; Champagnac et al. 2007) or Airy-type hydrostatic isostasy (e.g. Pari and Peltier 2000; Tong et al. 2007; Jadamec et al. 2007; Heine et al. 2008;) determined by characteristic local and sub-continental horizontal wavelengths, respectively. In this flexural approach, the juxtaposition of loads and anti-loads of variable size, the total deflection exceeds the linear Airy-isostatic response (first term on the right-hand side of Eq. 3.6) by a factor equivalent to the elastic response function (exponential term on the right-hand side of Eq. 3.6).

By considering the overall bending configuration in which the individual positive and negative loads (Fig. 3.2b) are superposed, our results display regional-scale vertical undulations of the lithosphere. Within the framework of the current study, we remain cognizant that flexural response to loading is but one mechanism to perturb the vertical configuration of the earth's solid outer surface.

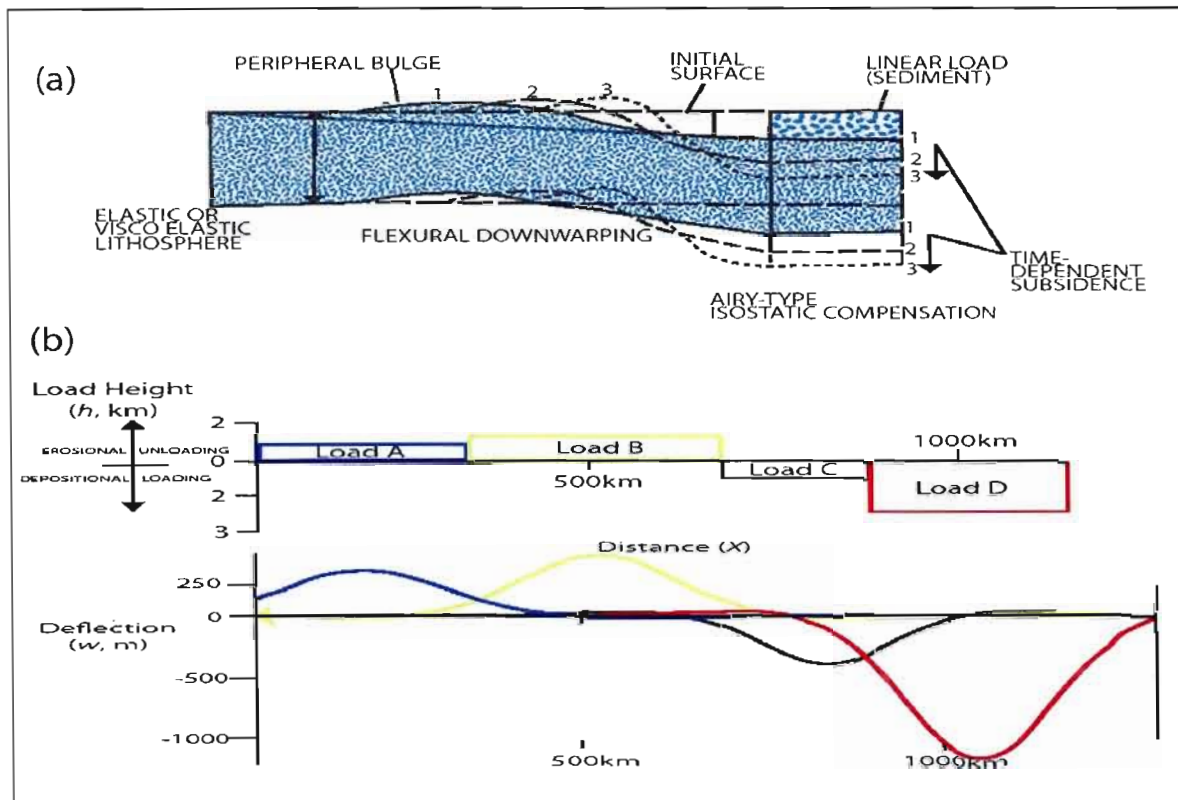


Figure 3.2 (a) Schematic illustration of both Airy-isostatic and flexural isostatic response(s) to sedimentary loading. The linear load is representative of sediments progressively filling a basin. Time-dependent subsidence is not necessarily required if the vertical response to all the loads are modeled as instantaneous. (Modified after Einsele 2000). (b) Typical two-dimensional configuration of four juxtaposed loads (upper) prescribed in this study and the magnitude of individual deflections (color coded, lower figure) based on Equation 3.6(a-c).

### 3.3 Mechanisms of Subsidence

How and why basins form is a central theme in earth science. Two main mechanisms are thought to drive the evolution of sedimentary basins. One is based on the fact that sediments, like water, travel to areas of minimum potential energy so, on long time scales, the ocean's basins become the repository for much of the terrestrial sediments (Milliman and Syvitski 1992; Hay 1998). Additionally, sediments may accumulate in regional topographic depressions. This creates a positive feedback system whereby sediment deposition invokes isostatically-driven subsidence (Watts 2001). Another mechanism involves a change in thermal regime where a cooling lithosphere contracts and increases in density, resulting in broad-scale subsidence (McKenzie 1978). This thermal subsidence can be invoked through crustal material alteration (Sleep 1971), or mineralogical phase changes, as well as crustal thinning by horizontal or vertical tectonic

mechanisms (Sclater and Christie 1980). An alternative source of subsidence revolves around the presence of density anomalies in the mantle as resolved through seismic tomography (Grand et al. 1997). Dense, negatively buoyant regions in mantle can impart enough stress on the lithosphere to create broad, relatively low amplitude depressions at the surface (Mitrovica et al. 1989; Forte et al. 1993). If initiated, the response by near surface mechanism, such as erosion and deposition, may further amplify the signal of subsidence.

### 3.4 Treatment of Anomalous Subsidence

Subsidence unaccounted for by an isostatic response to sediment accumulation or crustal structure is herein regarded as anomalous. In order to further constrain the magnitude of anomalous subsidence, flexural and isostatic response to loading and unloading is also considered. In what follows, stratigraphic distinctions coupled with a model datum surface allow for the extraction of geologically recent to modern patterns of subsidence. Using a multi-step approach, our goal is to isolate and quantify signals of anomalous neo-tectonic subsidence.

#### 3.4.1 Subsidence due to Sediment Loading

A stratigraphic distinction is first made between the two-layers of sediments as developed in CRUST2.0. The layer of hard sediments ( $c_4$ ) are presumed to represent a long-term history of sedimentation, erosion, burial, and diagenesis through numerous cycles of paleoenvironmental change. By contrast, the soft-sediment layer ( $c_3$ ) constitutes the material readily available for reworking and entrainment. In this way, the relative distribution of soft-sediments in and around the continents provide a general indication of sediment flux and regional depocenters.

In constraining neo-tectonic subsidence, we correct solely for the isostatic loading response ( $ISC$ ) of the hard sediments. This is quantified via empirically resolved density-depth relationships in marine sediments taking into account lithological variability, bathymetry and depth-dependent sediment densities (Sykes 1996; Segev et al. 2006);

$$ISC = 0.43422 \cdot t_s - 0.010395 \cdot t_s^2 \quad (3.7)$$

where  $t_s$  is the thickness of hard sediments in each column. The calculation restores, in a general way, the isostatic configuration of a sediment-free basement. Based on the stratigraphic distinction mentioned earlier, the layer 3 'in transit' cover sediments are treated separately in the effort to extract geologically recent signals of subsidence.

### 3.4.2 Subsidence due to Crustal Effects

Crustal heterogeneities can play an important role in the surface to near-surface geometry; so a correction for subsidence related to crustal structure is additionally required. The method used in this study stems from the derivation of isostatic surface topography (Eq. 3.3) described in Section 3.1.1. The differences here are: (1) along with the ice and water layers, the soft-sediment layer is additionally removed and, (2)  $\delta c_1$  is computed without including the load of soft-sediments;

$$H'_{iso} = \delta c_1 - c_1 - c_2 - c_3 \quad (3.8)$$

We thus restore the crust to its equilibrium isostatic configuration whereby the hard sediment layer comprise the solid outer surface ( $H'_{iso}$ ). This can be envisioned as a sort of paleodatum level, though only within our treatment of the model. It would otherwise have little or no stratigraphic relevance. By effectively omitting the soft sediments, we are able to prescribe our own local load configuration. In its simplicity, this approach neither requires knowledge of regional strain history, which is significant on longer time-scales, or parameters involving paleo-geothermics.

### 3.5 Anomalous Neo-Tectonic Subsidence

Anomalous Neotectonic Subsidence (*ANTS*) is quantified by subtracting the sediment corrected subsidence (*ISC*) from the paleodatum surface of the isostatically restored crust. ( $H'_{iso}$ );

$$ANTS = H'_{iso} - ISC \quad (3.9)$$

Obviously, the magnitude and spatial distribution of the anomalous subsidence field correlate with areas in the model overlain by soft-sediments. Incorporating the soft-sediment layer in the model formulation of ANTS would significantly increase the magnitudes of subsidence. The results are therefore considered lower-bound estimates. The study by Heine et al. (2008), which appropriately included total sediment thicknesses, was concerned with the long-term anomalous tectonic subsidence of very old interior basins, so their substantially higher estimates appear reasonable. By contrast, we focus on recent subsidence of major arterial regions draining significant continental areas.

#### 3.5.1 Basins with ANTS in Space and Time

Using the recent stratigraphic record and measured erosional parameters for selected basins with ANTS affinities, we further refine our approach by modeling the vertical response to sedimentary flux throughout the basins.

Preferential sediment deposition at epicontinental deltas create abrupt changes in sediment thickness from land to shallow sea that result in surface deflections both under and adjacent to the load. Using site-specific data on the thickness of sediment above well-constrained stratigraphic horizons within a delta, we quantify the effect of deltaic loads by modeling the related flexural response (Sect.3.2.2). The isostatic response to denudation is also considered for externally drained basins. By taking basin-wide denudation rates and integrating them over a characteristic time-scale (~3-5Mya), we also correct for vertical responses to the removal of

material by erosion. This is determined by using the sequence stratigraphic record of the basin's delta. To be consistent, the corresponding age of the sediments, used in the flexural analysis, is treated as a time-envelope for denudation. Anomalous neotectonic subsidence is now refined ( $ANTS'$ ) by including both a flexural correction ( $\omega_l$ ) for erosional unloading and depositional loading as well as isostatic rebound driven by denudation ( $D_{rbd}$ );

$$ANTS' = H'_{iso} - ISC - \omega_l - D_{rbd} \quad (3.10)$$

Results obtained from this approach will be particularly useful in isolating  $ANTS'$  for areas located subareally amid fluvial basins. By constraining these additional mechanisms, capable of affecting a basin's vertical configuration (Leeder 1991; Einsele 2000), a meaningful dynamic signal can be extracted.

### 3.6 Simplified Fluvial Modeling

Our depiction of fluvial systems reflects the tendency for material, over sufficient time scales, to emerge from a terrestrial basin into the marine environment. Upon sound interpretation of site-specific sedimentary field studies we are able to effect a sort of model 'front' that will either unload or add material to a given fluvial segment; essentially simulating denudation and intrabasin deposition, respectively.

## 4. RESULTS

### 4.1 Isostatic Topography

The isostatic topography field is derived from the crustal thickness and density structure of CRUST2.0 (Eq. 3.1-3.3). The configuration estimates the vertical amplitude by which the earth's solid outer surface would be deflected given an isostatically balanced crust (Fig. 4.1a). The range of values is similar to the observed topography, generally correlative with the bimodal nature of earth's hypsometry. However, the isostatic model predicts significantly higher elevations than those observed in many of the continental interiors.

#### 4.1.2 Residual or Non-Isostatic Topography of the Continents

Upon subtracting the calculated isostatic elevations from the observed topography we obtain the vertical relief unexplained by a crust-mantle lithosphere system in hydrostatic equilibrium (Eq. 3.4, Fig 4.1b). The values range between  $\sim +2\text{km}$  and  $\sim -2\text{km}$  capturing both the topographic and bathymetric envelope of mean terrestrial and marine elevations, respectively. The distribution of the observed elevations and the isostatic elevations are markedly different and alludes to a crust-lithosphere system out of hydrostatic equilibrium. A general pattern, though not without exceptions, emerges whereby negative values of residual topography are found within continental interiors. Positive residual topography is observed in some regions about the peripheries of the continents.

The map of residual topography clearly exposes the lateral distribution of current tectonic regimes amid the continents; thus, acquires geodynamic significance. Orogenic belts (e.g. Andes, Himalyas, Zagros) associated with active convergence display significant amplitudes of negative residual topography. This holds true, as well, for many intracontinental shields (e.g. Canadian, Guyana, Brazilian), cratons ( e.g. North American, Siberian, Congo) and related freshwater-brackish basins (e.g. Great Lakes, Hudson Bay, Lake Chad, Caspian Sea). Positive residual topography is associated with regions of active rifting (e.g East African Rift, Basin and Range) and their developmental progression from embryonic to narrow oceans (e.g., Red Sea, Lake Baikal). As well, high standing plateaus, some in the hinterland regions of cordilleras, (e.g. Altiplano-Puna, Colorado, Ethiopian) show some of the highest observed positive residual topographies.

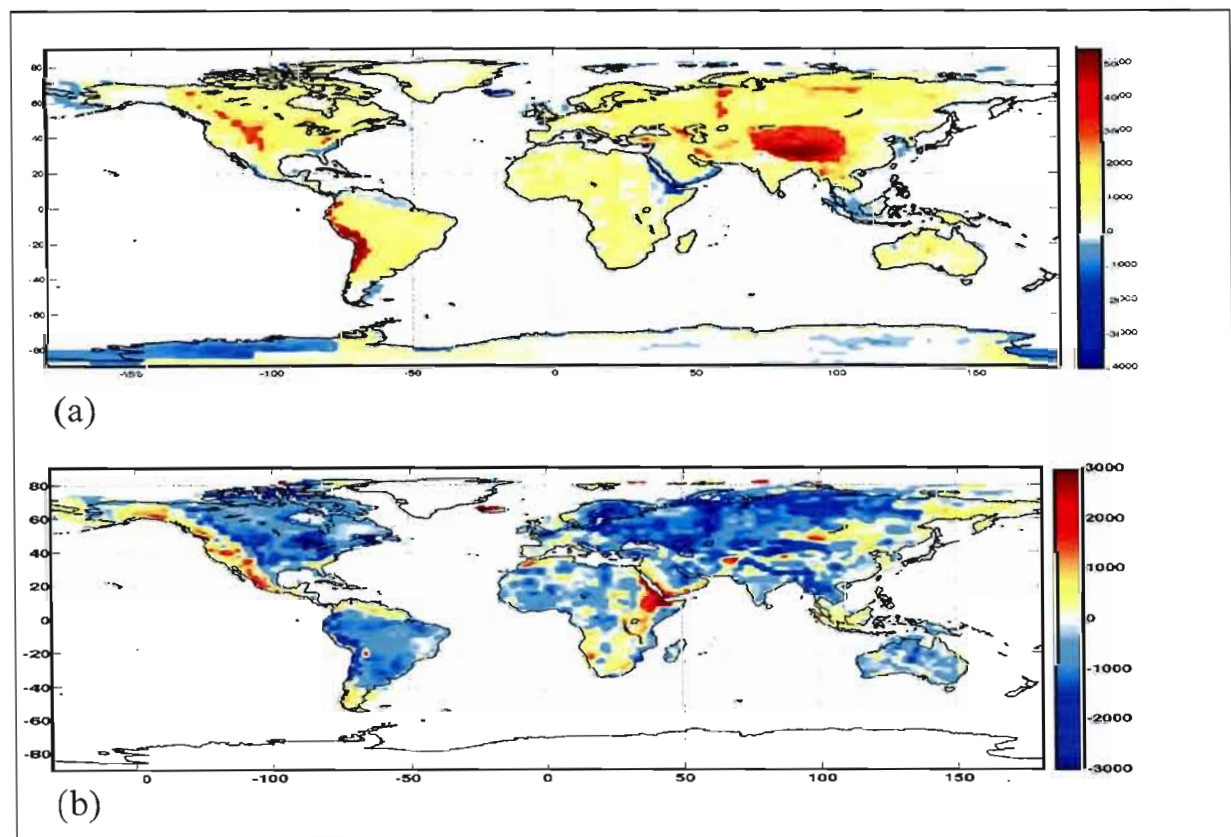


Figure 4.1 (a) Isostatic Topography (meters) of the continents based on the crustal and density structure of CRUST2.0. (b) The non-isostatic, or residual, topography (meters) field obtained from subtracting the isostatic elevations in (a) from the observed topography on the continents.

#### 4.2 Isostatic Restoration of Sedimentary Loads

The restoration of the basement configuration, constrained here by an isostatic correction to the layer-thickness of hard sediments, quantifies the vertical subsidence driven by sedimentary loading (Eq. 3.7, Fig. 4.2a). The observed values range from <0.1 km to 3.5 km.

Areas known to have protracted histories of sedimentation display thick sedimentary strata and are sites of marked depositions-driven subsidence. Not exclusively, many of these locales are situated sub-aerially about continental margins (e.g. Persian Gulf, Lower Mississippi Valley, Parahna Basin). Their positions are the very sites influenced by sea-level oscillations, major fluvial sedimentary dynamics, and paleo-environmental change. The other regions of significant sediment related subsidence are numerous intracratonic basins (Congo, Michigan, Chad) whose relative tectonic quiescence and longevity have established topographic depressions. Through time, such basins tend to spatially accommodate terrestrially derived detritus and preserve voluminous sedimentary sequences.

#### 4.2.1 Crustal Restoration Level

Modifying the formulation for the isostatic topography field (Eq. 3.8), we create a reference elevation field of a balanced crust devoid of soft sediments. This new elevation field (Fig. 4.2b) is conceived as a paleodatum-type surface whereby the crustal contribution to subsidence is measured. The restored crustal configuration is constrained to areas that have 200m or more of hard sediments. We are thus able to focus on regions having preserved significant amounts of sediments; presumably over long enough time-scales for burial-induced compaction.

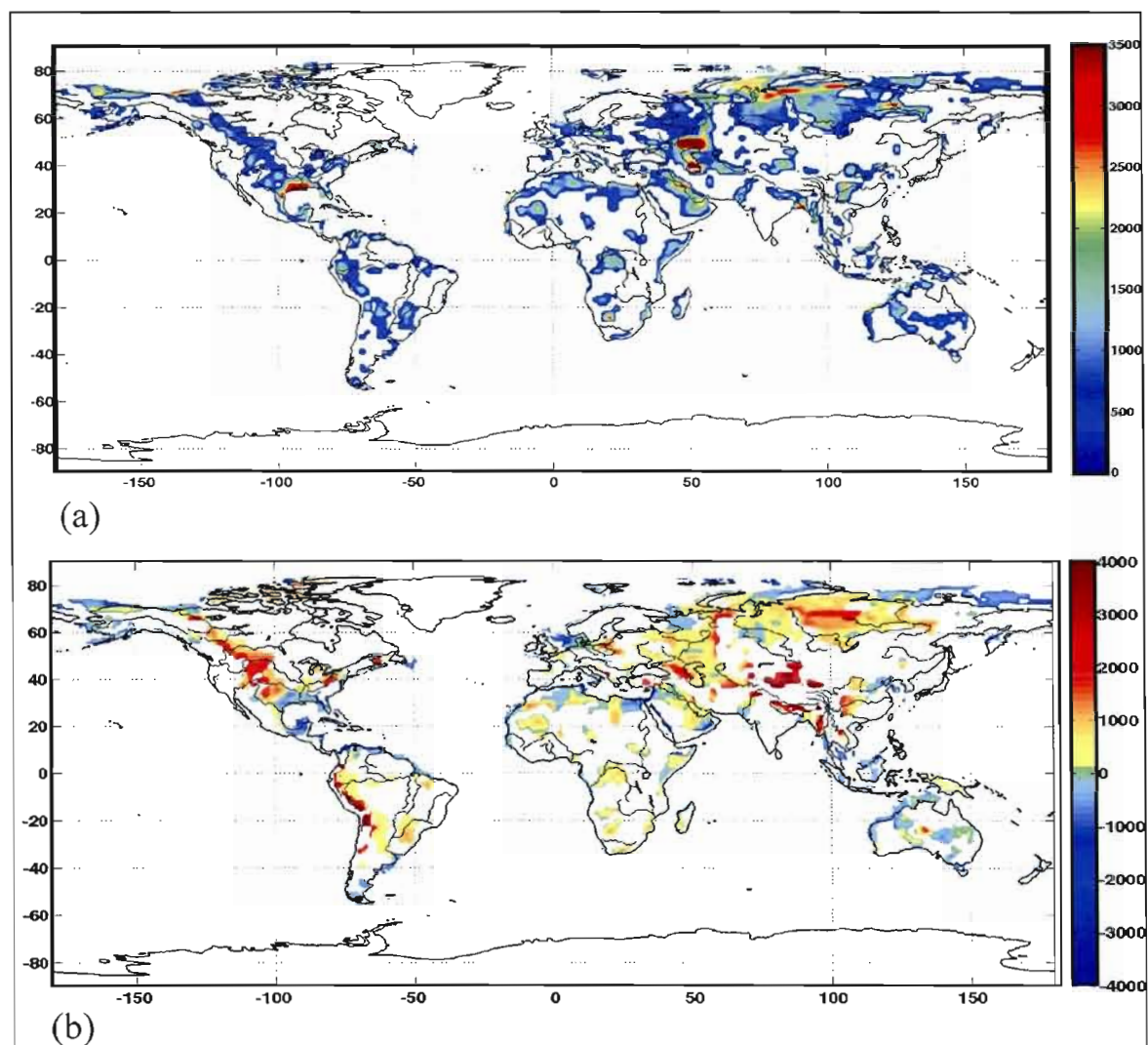


Figure 4.2 (a) Amplitude (meters) of sediment-load driven subsidence based on an isostatic correction, given in Eq. 3.4, applied to the layer thickness of soft sediments. (b) Isostatic Elevation field, or paleo-datum level, calculated here by restoring crustal columns to their equilibrium position without the soft sediment layer. Note: Continental areas that have less than 200m of hard sediments are excluded from the calculations.

The elevations of the paleodatum surface range from +4km - -4km about the continents. However, many of the values have amplitudes similar those of residual topography and tend to oscillate between +1.5km - -1.5km. Depressed regions are observed at the peripheries of several continents (e.g. SE United States, NE South America, N Africa). High-standing regions are found about the flanks of orogenic chains (e.g. Andes, Himalayas, Rockies) and adjacent to elevated plateaus (e.g. Colorado, Tibetan). A number of areas exhibit a quasi-concentric pattern of low negative amplitudes encompassing, and intercalated by, zones of low positive amplitudes.

### 4.3 Anomalous Neo-Tectonic Subsidence

The difference, or residual, between the subsidence values from the restored crustal configuration and those derived from sediment loading constitute the amplitudes of anomalous neotectonic subsidence (Eq. 3.9). Figure 4.3a represents patterns of ANTS for multiple continental catchment basins that contain >200m of hard sediments. The positive values are associated with the headwater source-regions of major river systems. High-amplitude negative values, ranging from -2km to ~-4km, are clearly associated with regions containing thick sedimentary sequences (E. Saudi Arabia, Mississippi Embayment). A general propensity for increasing negative ANTS from continental interiors to their margins is observed. This spatial pattern trends along major trunks of ocean-bound rivers (e.g, Mississippi, Tigris/Euphrates, Amazon). The distribution of significant negative ANTS are found within the lower reaches and debouchement of numerous rivers. They are located about the rivers' respective sub-aerial floodplains and deltas (e.g. Orinoco (Venezuela), Magdalena (Columbia), Nile (Egypt), Niger (Niger), Rio Grande (U.S./Mexico), Amazon (Brazil)). Negative ANTS is clearly associated with thick sedimentary sequences of variable depositional age as well as sites subjected to ongoing sedimentary dynamics at continental peripheries. We herein limit our study to regions of negative ANTS; this due to (1) inherent subsidence associated with basins and (2) their primary role as conduits of the geologically recent intracontinental sediment routing system.

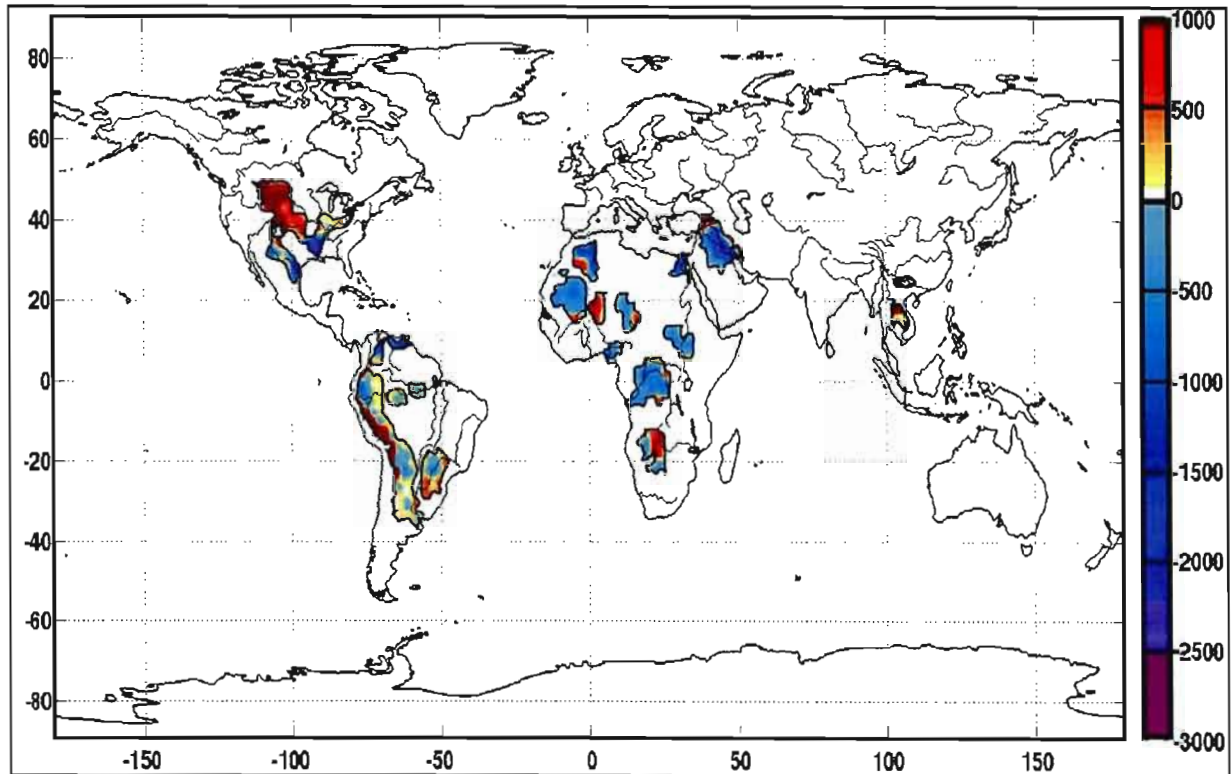
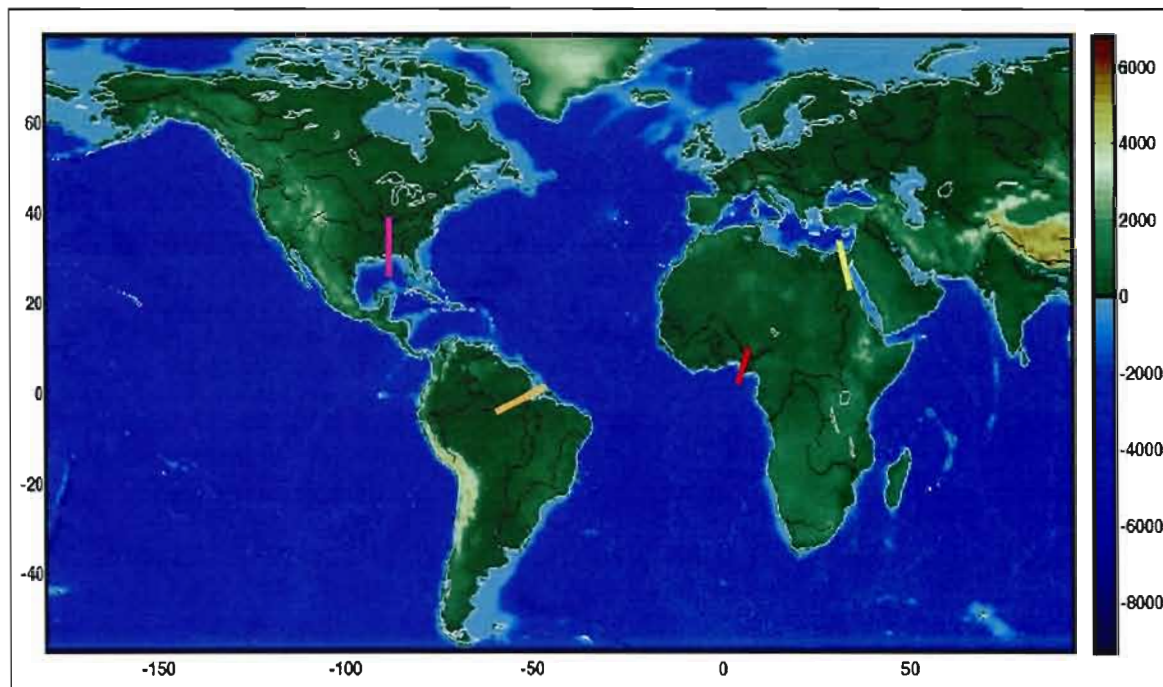


Figure 4.3 Anomalous neo-tectonic subsidence (ANTS, meters) for intrabasinal areas that host more than 200m of hard sediment. Note the increasingly negative values of ANTS towards the basins' rivers respective ocean-proximal outlets.

#### 4.4 Flexural Response to Erosion and Deposition

To optimize our isolation of what we believe to be anomalous subsidence, additional corrections are made for the flexural response to fluvial incision and submarine deposition at continental margins (Eqs. 3.5 and 3.6). The anomalous neo-tectonic subsidence observed in many modern drainage basins leads to our selection of four river basins where geologically recent to modern sedimentary dynamics can be studied. The chosen rivers (Fig 4.4) are: (1) Nile River, (2) Amazon River, (3) Mississippi River and, (4) Niger River. These rivers, and their bounding basins, are geographically and geomorphologically distinct from each other as well as having unique sedimentation histories. Our goal is not to differentiate the rivers but rather to assess their respective geological settings and dynamic histories to obtain meaningful results within a geodynamic framework.



Figure

4.4 ETOPO2 DEM with selected lower-reach river segments used in flexural modeling (pink, Mississippi River; orange, Amazon River; red, Niger/Benue River; yellow, Nile River).

#### 4.4.1 Input Parameters

Table 4.1 lists the input parameters for the two-dimensional flexural response models. Transect lineation is generally parallel to the considered river segment. Based on a thorough review of the literature, we divide each transect (Fig 4.4) into segments where erosional unloading or depositional loading are imposed (*see* Appendix 1 and Appendix 2 for plan-view and cross-sectional imposed loading architectures). The inland segments, often starting at major river confluences or at the edge of an interior basin are characterized by varying amounts of sub-aerial erosion. Approximately a quarter of the transect distance extends into the marine realm and contains the thickest sedimentary deposits and model loads. The interim segments, comprising more than half the transect lengths, are prescribed as either erosional unloading or depositional loading. The latter tends to increase in amplitude as the model loads propagates towards the coast (*see* A. 2). The maximum age of these submarine sequences, derived from the Miocene-Recent biostratigraphic records, define our time-envelopes for each basin (*see* Sect. 3.5).

#### 4.4.2 Flexural Model Results

The prescribed rectangular loading configurations and the associated flexural responses (Eq. 3.6) are shown in Figure 4.5. A quadratic fit to the load geometry is made after the flexural response is established. We prefer the visibly smooth representation as it captures the modulating nature of surface processes within low relief terrains: hillslope processes, basin fill geometry, and degradation of ancient orogens have been modeled using the diffusion transport equation (e.g. Pelletier 2008; Stuwe 2007; Turcotte and Schubert 2001)). Thus, where erosion is to some degree proportional to the curvature of the terrain, a low-frequency graphical depiction is rather suitable.

Table 4.1 Flexural and Loading Input Parameters

River/Basin - Legs -Sub-basins	Elastic Thick. <sup>(ref)</sup>	Transect Coordinates(deg.) (Lat1, Lon1) (Lat2, Lon2)	Transect Distance (km)	Height <sup>(ref)</sup> of Erosional Unloading <sup>o</sup> (horz.dist.)	Height <sup>(ref)</sup> of Depositional Load <sup>o</sup> (horz.dist.)	Maximum Geological Era <sup>(ref)</sup> (age)
Nile	25 km <sup>(14)</sup>	28.5°N 32°E 37.5°N 34°E	~1200km			
-Lake Nasser					0.5km <sup>(100km)</sup>	Latest Miocene <sup>(6)</sup>
-Eastern Desert				0.2km <sup>(2-3)</sup> (300km)		(5.8Mya)
-El-Minia - Cairo				0.6km <sup>(2-3)</sup> (400km)		
-Cairo-Med.Coast				1.2km <sup>(2-4)</sup> (300km)		
-SE Med. Basin					3.5km <sup>(20)</sup> (200km)	
Amazon	35 km <sup>(7)</sup>	7°S 60°W 2°N 45°W	~1400km			
-Solimas Basin					0.5km(100km)	Pliocene <sup>(9)</sup>
-Manaus-Santarem				0.75km <sup>(4)</sup> (400km)		(5 Mya)
-Santarem-Gurupa				1.0km <sup>(8)</sup> (500km)		
-Gurupa- Ati.Coast					1.2km <sup>(2)</sup> (100km)	
-Offshore W.Atlantic					2.6km <sup>(2)</sup> (200km)	
Mississippi	35km <sup>(10)</sup>	37°N 83°W 28.5°N 85°W	~1150km			
-S. Illinois Basin					0.5km <sup>(14)</sup>	Early Pliocene <sup>(13)</sup>
-N. Madrid-to- ArkansasR./Miss.R				0.75km <sup>(13)</sup> (400km)		(4.75 Mya)
-N-S Macon Ridge				1.15km <sup>(12)</sup> (200km)		
-Gulf Coast					0.16km <sup>(11,14)</sup> (300km)	
-Offshore Gulf					3.6km <sup>(11,14)</sup> (250km)	
Niger	30km <sup>(15)</sup>	2.2°N 7.5°E 5.5°N 11.5°E	~600km			
-Niger R./ Benue R.				0.25(200km)		Latest Miocene <sup>(17)</sup>
-N-S Benue Lineament					2.1km <sup>(20)</sup> (200km)	(6 Mya)
-Offshore E.Atlantic					3.5km <sup>(17)</sup> (200km)	

References: 1. Govers et al. (2009); 2. Woodward et al. (2007); 3. Said (1981); 4. Mahmoudi and Gabr (2009); 5. Segev et al. (2006); 6. Abu El-Ella (1990); 7. Perez-Gussinye et al. (2007); 8. Costa et al. (2001); 9. Figueredo et al. (2009); 10. Blum et al. (2008); 11. Shunk et al. (2006); 12. Van Arsdale et al. (2007); 13. Weimer (1990); 14. Crouch (1959); 15. Hospers (1965); 16. Cohen and McClay (1996); 17. Whiteman (1982)

$$a. \rho = \frac{\rho_s}{\rho_m}$$

$$b. \rho = \frac{(\rho_m - \rho_w)}{\rho_m}$$

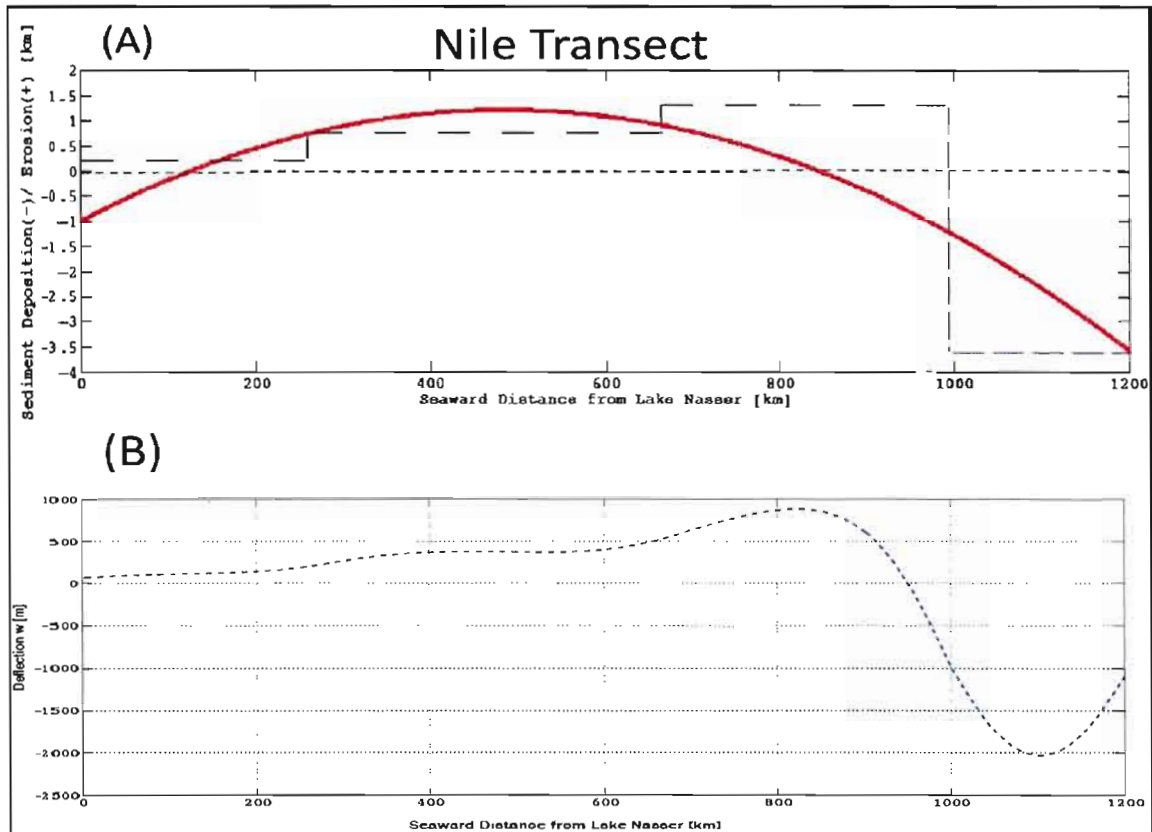


Figure 4.5. (A,C,E,G) Imposed anti-loads (erosional unloading, black dashed) and loads (depositional loading, dashed purple) distributed across transects listed in Table 4.1. The thick red curve is a smooth quadratic fit to the model loading/unloading. This was fitted after the vertical deflection (in meters), or flexural isostatic response, is simulated (blue-dashed lines depicted in B,D,F,H) using Eq. 2.5

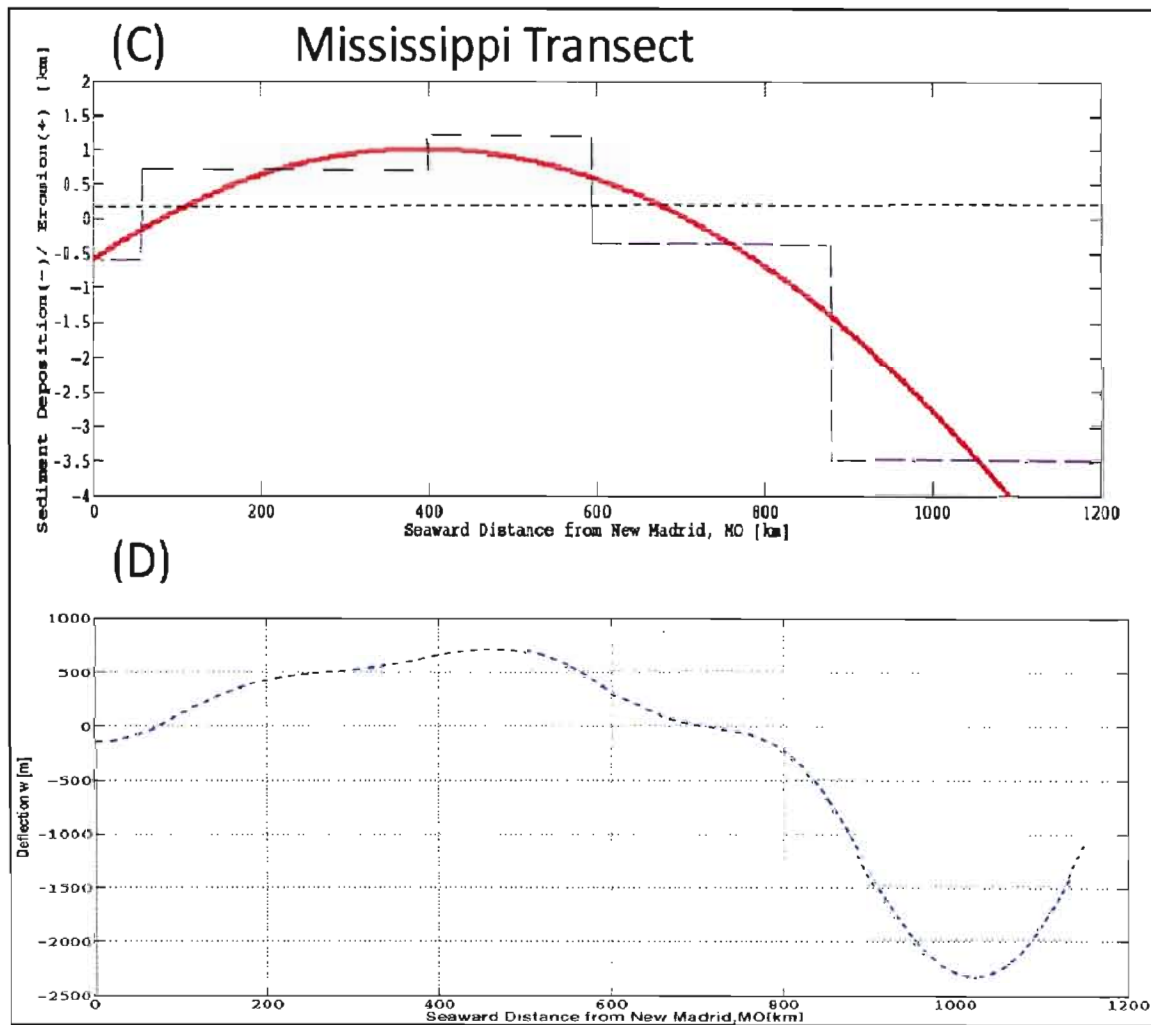


Figure 4.5 cont'd

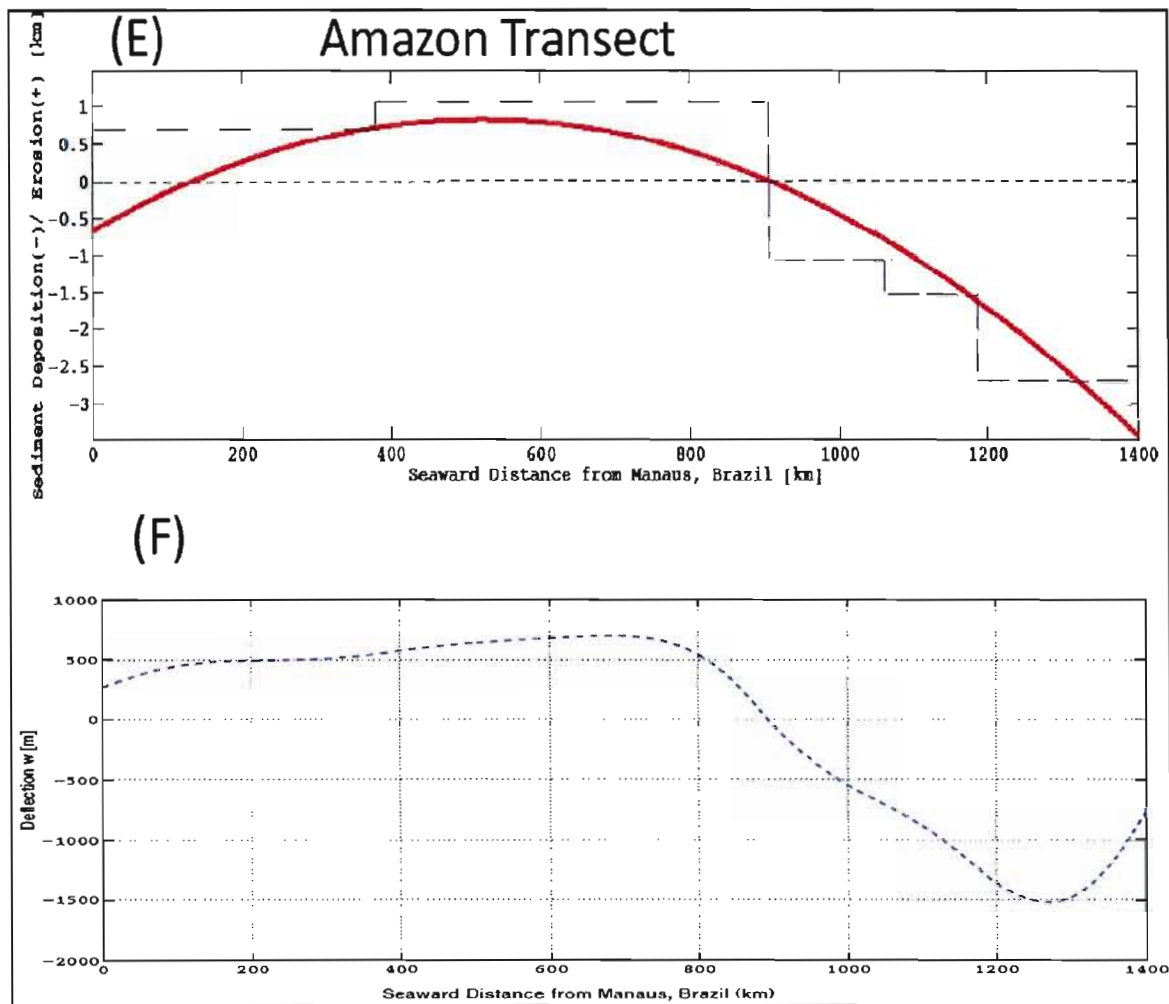


Figure 4.5 cont'd

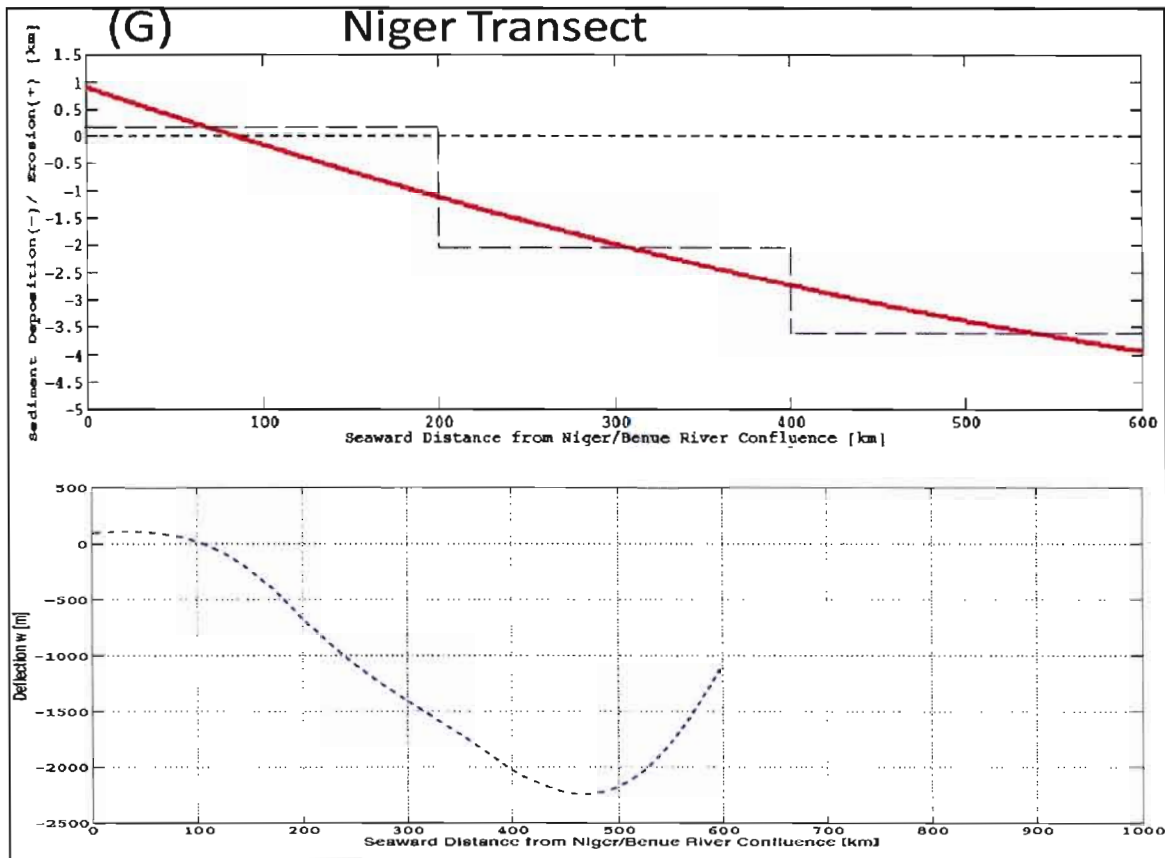


Figure 4.5 cont'd

Modeled flexural responses of the selected basins show how the force system imparted by thick sedimentary loads, observed in the off-shore, dominates the regional flexural signal. The overall effect is a downwarping of the sub-aerial lower reaches of ocean-bound river channels and shore-proximal basin regions (*see* A1 and A2). The observed inland positive deflections are substantially subdued compared to negative the flexural signal. Flexural uplift is generated by the coupled effects of prescribed erosional unloading and upward deflection, or bulging, in response to rather large far-field deltaic depositional load (e.g. Beaumont 1981; Quinlan and Beaumont 1994).

Table 4.2 lists the vertical deflections and their spatial extent for each river system. The values are areally weighted to derive a single flexural correction for the terrestrial portion of the basin. The distance and magnitude over which the deflections change polarity is also tabulated. The sign for these inflection segments are negative because we measure flexure in the direction

of the greatest positive load. Clearly, these are the off-shore deposits comprising each basins' respective submarine fans.

Table 4.2. Summary of Vertical Flexural Responses at Key Inflection Points

River/Basin	Mean Flexural Response to Sub-Aerial Erosion <sup>a</sup>	Transect Segment (km)	Sub-Aerial Flexural Response to Deposition <sup>b</sup>	Transect Segment (km)
<b>Nile</b>	+500m	800km (Aswan-Cairo)	-1000 m (Cairo-Med. Shore)	200 km
<b>Amazon</b>	+600m	900km (Manaus-Gurupa Arch)	-1400m (Marapo Basin)	300km
<b>Mississippi</b>	+400m	700km (N.Madrid-S.Macon Ridge)	-1300m (S. Macon Ridge – Gulf Coast)	300km
<b>Niger</b>	-600m	300km (Lower Niger River)	-1750m (Niger Delta Plain)	100km

a. Areally weighted across the terrestrial portions of transects

b. See Table 4.1 footnote b. Note this will be subtracted from ANTS to correct for the flexural isostatic component of subsidence

Table 4.3 Denudational Corrections

River/Basin	Denudation Rate <sup>c</sup>	Elapsed Time <sup>a</sup>	Height ( $X$ ) of Eroded Material	Isostatic Response ( $\Delta h$ , Uplift) to Denudation <sup>b</sup>
Nile	18mm/kya	5.8 Mya	104 m	42m
Amazon	90mm/kya	5 Mya	450 m	182m
Mississippi	70mm/kya	4.75 Mya	330 m	134m
Niger	10mm/kya	6 Mya	60m	25m

a. Time envelope derived from offshore sequence stratigraphic records (see references cited in Table 4.1)

b.  $\Delta h = X \frac{(\rho_m - \rho_f)}{\rho_m}$  (Stuwe 2007; Allen and Allen 2005)

c. Data from basin-wide average denudation rates compiled by Summerfield and Hulton (1994)

#### 4.5 Denudational Isostatic Uplift

The final correction applied to the ANTS observed for the selected river basins is the isostatic response to denudation. Historically, this parameter has almost exclusively been employed on smaller scales within mountainous regions (e.g. Montgomery 1994, Tong et al. 2007, Stuwe 2007). However, we feel its simple appropriation will additionally constrain subsidence currently unexplained, now, by: (1) sediment loading, (2) crustal configuration, (3) erosion/depositional driven flexure (Table 4.4).

Using the basin-wide rates of denudation from the compilation of Summerfield and Hulton (1994) integrated over an elapsed time we obtain a first order height estimate of eroded material. The isostatic response to material unloading is computed to simulate isostatic rebound and associated vertical uplift due to basin-wide erosion. The scheme is shown in Table 4.3. Obviously, the amplitudes will scale with the denudation rate since our time envelopes are

generally from the Pliocene Era (post-Miocene) onwards. Adding this correction to the values of ANTS becomes quite significant for shore-proximal regions of the Amazon and Mississippi basins. Though the correction is substantially less for the Nile and Niger basins, they are certainly not negligible with regard to the temporal scales and dynamics addressed in this study.

#### 4.6 Corrected Anomalous Neo-Tectonic Subsidence (ANTS')

The corrected anomalous neo-tectonic subsidence (Eq. 3.10) for the selected basins and their respective major river trunks show marked amplitudes unaccounted by the geological parameters addressed in this study. Basin-wide results are summarized in Table 4.4. Sub-aerial intrabasinal distribution of ANTS' is mapped in Figure 4.6.

Importantly, only the shore-proximal areas of the selected basins include flexural effects (*see* Appendix 1) rendered from our calculations of corrected anomalous neotectonic subsidence. Naturally, then, the highest amplitudes are observed about these localities: E.g. the Egyptian Nile and the Lower Mississippi River are systematically depressed by  $-1.5 \text{ km} \pm 250\text{m}$ . A notable exception, being positive ANTS', can be found in the Guruapa portion (*see* Table 4.1) of the Lowermost Amazon.

The subdued amplitudes, both positive and negative, observed in the upper reaches and catchment boundaries of each fluvial basin is a direct result of the methodology followed in this study. Again, flexural corrections are only made about the lower reaches of each fluvial system. Inland source regions, due to our methodology, remain less affected. For example, the greater northwest region of the Mississippi Catchment (Great Plains, Western Cordillera) and the inland portions of the Niger River system (the Guinea Highlands in Mali, Southwest Niger) reveal elevations in excess of  $\sim +500$  meters. In Africa, the Sudd floodplain (Southern Sudan), West Chad, and Mauritania into Southern Nigeria show several hundred meters of anomalous negative subsidence.

The corrected ANTS (ANTS') for the selected basins, and their respective trunk rivers, reveal a bimodal distribution of subsidence values unaccounted for by the parameters addressed in this study. The Mississippi and Nile drainage basins show approx. -1.5km of subsidence. The subsidence associated with the Amazon and Niger drainage basins oscillate about -200m. Basin-wide results for the four variables (ISC,  $H'_{iso}$ ,  $w(x)$ ,  $D_{rbd}$ ) are summarized in Table 4.4. The sub-aerial intrabasinal distribution of ANTS' (Eq 3.10) is mapped in Figure 4.6.

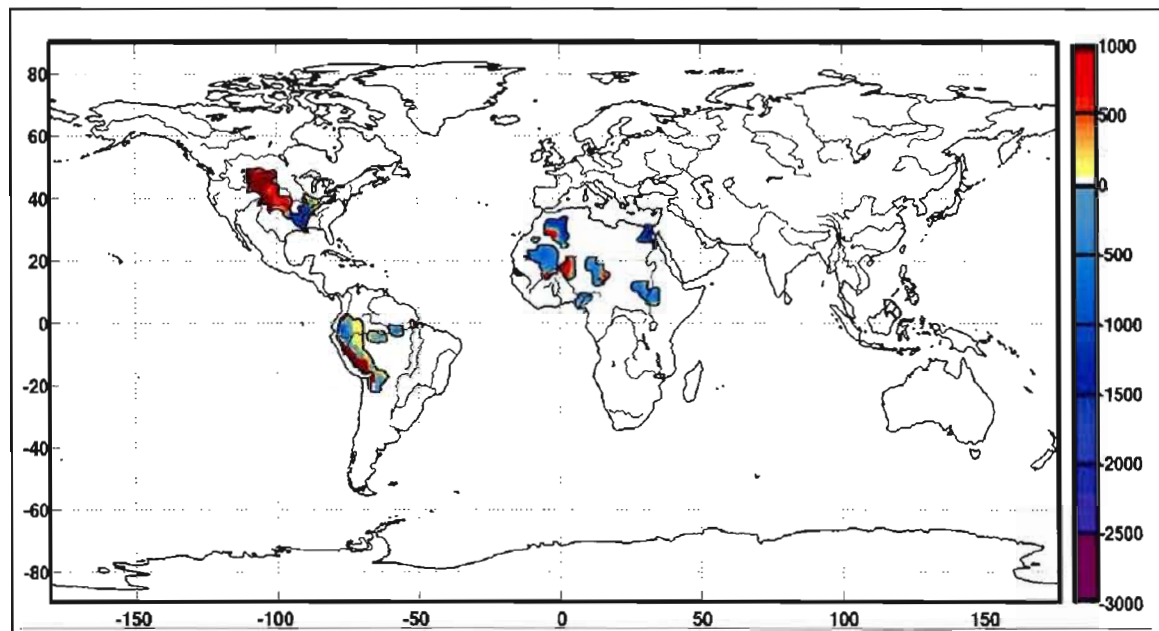


Figure 4.6. Anomalous neo-tectonic subsidence corrected for sediment loading, crustal configuration, erosion/depositional driven flexure and isostatic rebound to basin-wide erosion. See text analysis and explanation

Table 4.4 Summary of corrected parameters applied to Anomalous Neo-Tectonic Subsidence

River/Basin	Subsidence due sediment loading ( <i>ISC</i> )	Subsidence related to crustal restoration ( <i>H'iso</i> )	Uncorrected Anomalous Neo-Tectonic Subsidence ( <i>ANTS</i> )	Flexural Isostatic Correction ( $w(x)$ ) (Leg1, Leg2) <sup>a</sup>	Isostatic Rebound to Denudation
<b>Nile</b>	~ 0.7km	~ -.8km	~ -1.5km	~ +0.5 km, -1km	~ 0.04km
<b>Amazon</b>	~ 0.7km	~ -0.5km	~ -0.12km	~ +0.6km, -1.4km	~0.180km
<b>Mississippi</b>	~1.7km	~ -0.7km	~ -2.4km	~ +0.6km, -1.3km	~ 0.134km
<b>Niger</b>	~1.0km	~ -0.3km	~ -1.3km	~ -0.6km, -1.75km	~ 0.025km

a. Leg1 ~ shore proximal segment; Leg 2 ~ middle/inland river reaches

## 5. Discussion

The current study has shown the existence of geologically recent to modern anomalous subsidence (ANTS') associated with several major continental drainage systems. We constrain our study to four basins and their ocean-bound major arterial rivers. However, the same methodology could theoretically be applied to many, if not all, of the world's major terrestrial drainage basins.

The choice to focus on the Nile, Mississippi, Amazon, and Niger River basins emanated from the conventional view that they are positioned within relatively stable continental regions and ocean margins. We presently explore the relationship, if any, between mantle dynamics and active fluvial systems. The Pliocene-Recent geomorphological and neotectonic history of each region is briefly discussed in which we present each basin's general structural lithostratigraphy and setting depicted in Figure 5.1. Signals of ANTS for each basin are considered with respect to near-surface gross architecture, geophysical observables, and global geodynamic predictions. Establishing the extent to which basin scale features and dynamics relate to deep-earth processes provides a context for fluvial and sediment routing systems within a geodynamic framework.

### 5.1 Physiography of the Nile River Basin

The Nile is the world's longest river, >6500km, with a drainage area up to  $3 \times 10^6$  km<sup>2</sup>. Sources of sediment delivered to the Mediterranean via the Nile come mostly from interior regions farther than 2700 km south of the Egyptian coast (Woodward et al. 2007). The north-flowing east equatorial White and the northwest-flowing Ethiopian Blue Nile carry cratonic quartz-rich sands and mafic-volcanic muds, respectively, from the highlands of Africa (Garzanti et al. 2006). Middle 'African' and the lower 'Egyptian' reaches of the Nile cross the Sudd floodplain of central Sudan into the arid deserts of Egypt where they converge at the sub-aerial, V-shaped Nile Delta and east Mediterranean Basin.

#### 5.1.1 Structural Features of the Nile in Northern Sudan and Egypt

The Pre-Cambrian NNW-SSE trending Dongala-Salima rift zone, and associated tectonic fabric, guide the African Nile into the Lake Nasser area of southern Egypt (Abdelsalam and Stern 1996). North of Aswan a small stretch of the Nile meanders towards the east traversing the E-W trending Kom-Ombo graben (El-Bastaway et al. 2010). Over a relatively short distance, the Nile regains its northward course into Cairo

within an incised, scarp-bounded topographic low (Albritton et al. 1990, Fig. 10). Bounded to the south by north dipping fault segments, most of the ~200 km sub-aerial delta occupies a structural downwarp zone representing a continental margin related depression (Sigaeiv 1959).

### 5.1.2 Late Miocene to Recent Egyptian Nile Basin Sedimentary Dynamics

The most prominent event in the Egyptian Nile Basin's stratigraphic record, marked by a sub-surface erosional unconformity, is the purported Messinian (Late Miocene) Salinity Crisis; where the entire Mediterranean Sea was cut off from its connection to the Atlantic (e.g. Loget and Van Den Driessche 2006). Rapid evaporation resulted in both the deposition of thick salt strata atop the desiccated basin as well a deep fluvially-incised canyon system extending from interior Egypt into the southeast Mediterranean Basin (Ryan 1977; Gargiani et al. 2010). Depositional infilling of the ~1 km deep (see Table 4.1) Nile Canyon and subsequent marine regression characterizes the stratigraphic record of the Egyptian Nile River Basin.

Following Zaki (2007), paleo-environmental evolution towards the modern fluvial setting is as follows: (1) Early Pliocene marine transgression flooded the existing gorges depositing shallow marine sediments. (2) Late Pliocene regression created an estuarine setting from Aswan to the Mediterranean. (3) From Pleistocene onwards, the deposits of the Egyptian Nile consist of mixed fluvial and lacustrine sediments derived from the modern day source regions (see Section 5.1) and the Eastern Desert, respectively.

## 5.2 Physiography of the Amazon River Basin

The present-day Amazon basin is intimately related to Andean uplift and the ongoing convergence between the Nazca and South American tectonic plates (Iaffaladano et al. 2006; Garziona et al. 2008; Forte et al. 2010). Draining an area greater than  $7 \times 10^6$  km<sup>2</sup>, the continental-scale Amazon basin contains numerous and diverse large river systems sourced by the Andean orogenic chain to the west, the Guiana and Brazilian Shields to the north and south, respectively, (Mertes and Dunne 2007).

Major tributaries converge upon the ENE trending Amazon River system comprising three river segments and associated sub-basins. From western interior Brazil to the Atlantic Ocean they are: The Solimoes, Peru, and Amazon segments. The collective sedimentary loads that reach the Atlantic Basin form the deposits of the shore-proximal shelf and Amazon Cone.

### 5.2.1 Structure

The main trunk of the Amazon River system flows within the pre-Ordovician ENE-trending Amazon suture that separates the Guiana and Brazilian Shields (Sengor and Natal'in 2001). Recent studies have shown the effective elastic thickness of the suture zone to be nearly one-third of the values of the adjacent shields (Perez-Gussinye et al. 2007). This supports the idea that fluvial segments flow within regions of existent or inherited crustal weakness (e.g. Potter 1978; Abdelsam and Stern 1996; Miall 2007). Within the suture zone, the sub-basins of the Amazon (Sect. 5.2) are bound by the N-S trending structural highs of the Jutai, Purus and Guarapa Arches (Costa et al. 2001).

### 5.2.2 Late Miocene to recent Sedimentary Dynamics of the Amazon River

Late Miocene to Early Pliocene depositional setting of the Solimoes basin (a.k.a East Amazon Basin) near the Purus Arch (*see* A.1) is interpreted as either tidally influenced megalacustrine (Frailey et al. 1984) or shallow marine deposits (Roddaz et al. 2006). Whether there existed an interior sea, a connection to the Atlantic, or a very large lake, the Solimoes Basin was likely a regional depocenter in the Early Pliocene. From the Late Pliocene to recent, the basin setting evolved from floodplain, lacustrine, to its modern fluvial architecture (Roddaz 2006; Costa et al. 2001).

Aside from the ~200m and ~700m fluvio-lacustrine sediments within the western Purus Basin and eastern Amazon Basin, respectively, the Late Pliocene to Recent history of the two segments is characterized by fluvial incision into, and denudation of, Cretaceous sediments (Costa et al. 2001); thus establishing the observed erosional planation surface (unconformity,

A.1). Although sea-level fluctuations over the last 5 My have certainly affected sedimentation from the Purus Arch seaward (Vital and Stattegger 2000), the marked increase in clastic deposition upon the Amazon Fan (Figueiredo et al. 2009), perhaps on pace with the growth of the Andes, indicates significant entrenchment of the lower Amazon River since the earliest Pliocene.

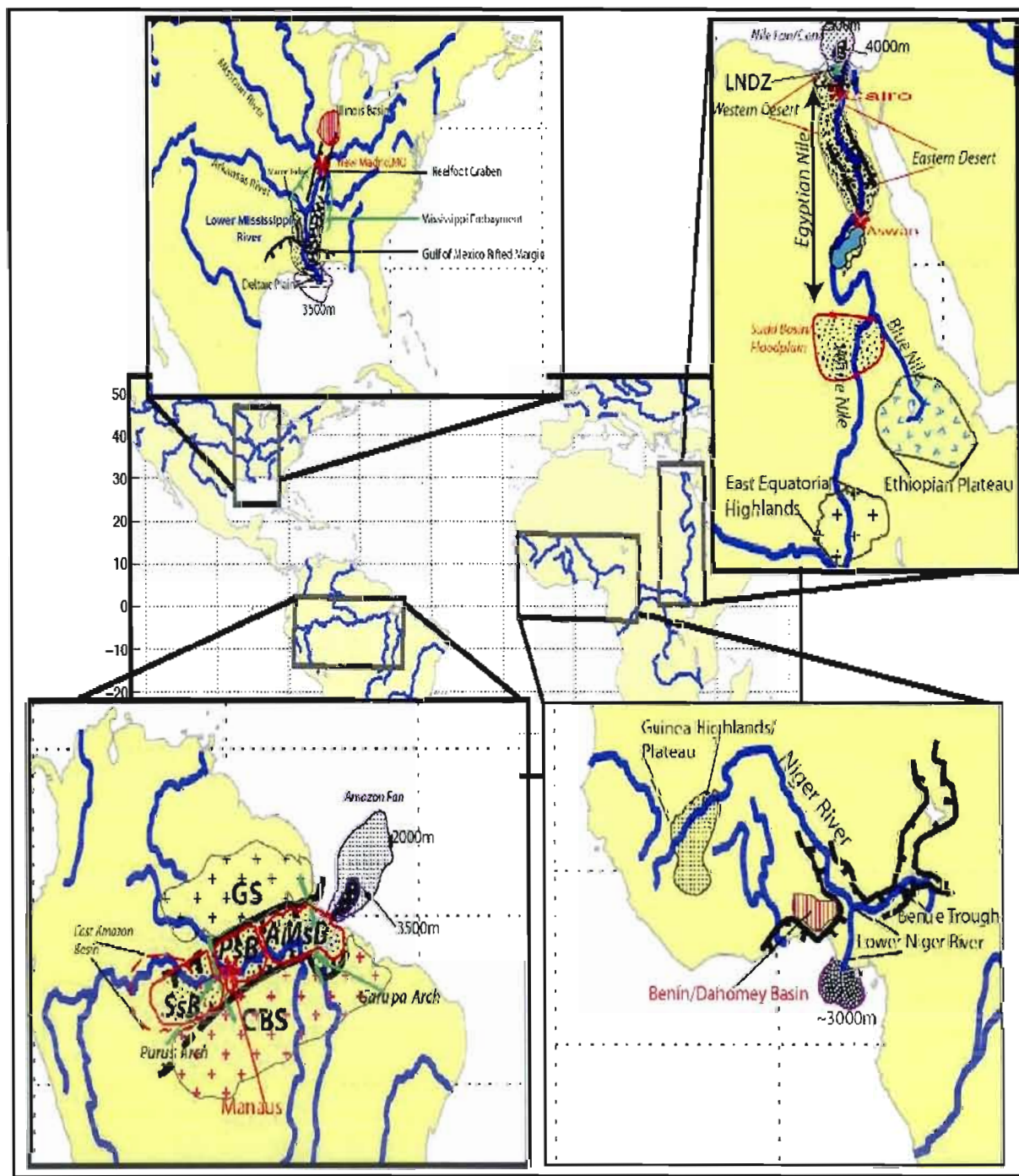
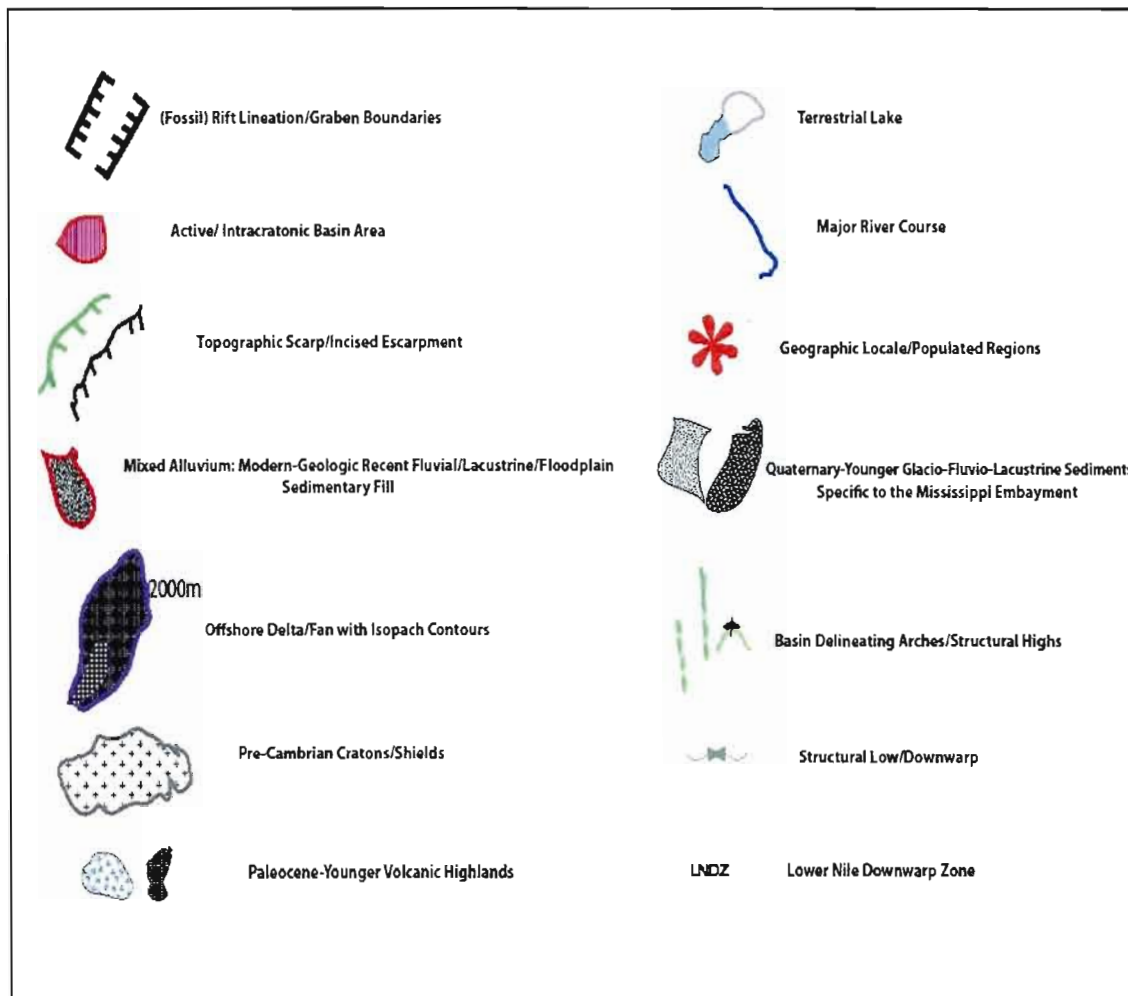


Figure 5.1 Physiographic map compilation of the four basins addressed in this study. Features include general surface lithological facies, geomorphic and sedimentary environments, river bounding fault lineaments, key physiographic and geographic locales, and approximate morphometry and sediment isopachs of each fluvial system's respective offshore deltas and fans. Legend contains the various symbols and keys depicted in the planview map. SsB - Solimoes sub-Basin, PsB - Purus sub-Basin, AMsB - Amazonia sub-Basin, GS - Guyana Shield, CBS - Central Brazilian Shield. See text for a brief description of each basin's lithostratigraphy, gross architecture and structural geology. Included in our discourse is a review of previous work that focused on the Pliocene-Recent sedimentological evolution of the fluvial basins, and their major ocean outlets, discussed in the current study.



### 5.3 Physiography of the Mississippi Embayment

Close to 75% of the  $3.2 \times 10^6$  km<sup>2</sup> Mississippi basin drainage area is located north of the Lower Mississippi River and Embayment. Sedimentary loads and fluvial discharge are

predominantly delivered by the Rocky Mountains, via the Great Plain states, of the Missouri and east-central U.S Ohio River systems, respectively (Knox 2007). South of the Illinois Basin and Missouri River confluence, the Mississippi flows southward to form a river-dominated delta in southern Louisiana and debouche into the northeastern Gulf of Mexico.

### 5.3.1 Regional Structure

Near the northern limit (New Madrid, MO) of the Mississippi Embayment, the south-flowing Mississippi River is situated within the NE-SW trending fault pair of the Early-Middle Cambrian Reelfoot graben. The Mississippi Embayment is delineated by a bell-shaped scarp whose northern apex is located near Cairo, Illinois. To the south, the mid-Paleozoic Appalachian/Ouachita thrust front (Harry and Londono 2004), reversely reactivated in the Late Triassic to Early Jurassic, dominates the architecture of the east-west Gulf of Mexico rifted margin (Sengor and Natal'in 2001). Since the Late Cretaceous, this region is believed to occupy a zone of broad crustal down-warping (Knox 2007). The course of the Mississippi River's lowermost reach is constrained to the east by the locally elevated Macon Ridge Complex and to the west by Pleistocene (Blum et al. 2008) sedimentary deposits.

### 5.3.2 Pliocene to Recent Sedimentary Dynamics of the Lower Mississippi River

Thick, southward progradating Plio-Pleistocene sedimentary sequences observed in the northern Gulf of Mexico is evidence for a rapid increase in deposition of terrestrial material since the Early Pliocene (Woodbury et al. 1973; Weimer 1990).

In the Mississippi River Valley area, from New Madrid to the confluence of the Arkansas River, the Pliocene environment was similar to the present-day setting. The main trunk flowed southward, depositing clastic sediments to form a broad forested floodplain. However, fluvial

gravels situated on modern day, ~100m high, ridge-tops are believed to be stranded strath terraces of the paleo-river (Van Arsdale 2007). Base-level fall and Quaternary glacial meltwater cycles (Blum et al. 2008) caused the Mississippi River to incise the landscape, effectively lowering the surface on which it flows, influencing the delta plain architecture within modern-day Louisiana (Einsele 2000). Notably, regional subsidence has been reported for the northern Gulf of Mexico (Dokka et al. 2006) so the exact tectonic framework and associated fluvial response remains somewhat unresolved.

#### 5.4 Physiography of the Niger River Basin

The greater Niger Basin, from Graham et al. (1999), covers much of interior west-central Africa. Since the Niger/Benue segments are the sole arteries to the east equatorial Atlantic, the following geomorphic, structural, and sedimentological description of the Niger River Basin is limited to the catchment boundaries represented in Summerfield and Hulton (1994) (Fig 2.4).

The Niger River Basin, herein, encompasses the Niger River segments within eastern Guinea, southern Mali, west Nigeria, and most of Niger. The drainage area reaches  $2 \times 10^6$  km<sup>2</sup>, comprised in the most part by the Guinea shield. Unlike the other rivers considered in this study, the headwaters of Niger River are only 250-300km from the Atlantic shore. The major source regions are found within Liberia, Sierra Leone, and the 800m high Guinea Plateau. Following a broad arc-shape course, the Niger River flows northeastward from the tropical highlands of Guinea, turns southeast about Mali, and finally converges with the E-W Benue segment to flow 400km south until reaching the Atlantic.

##### 5.4.1 Regional Structure of the Niger River Basin

Located within a large aulacogen, the middle and lower reaches of the northwestern, northeastern, central, of the Niger River system follow the triple-arm architecture of the Aptian-Albian aged Bida, Douala, Benue Troughs, respectively (Sengor and Natal'in 2001). The

southernmost Atlantic-bound segment of the Niger River flows parallel to the eastern edge of Benin's Togo-Dehomey shore-proximal basin.

#### 5.4.2 Late Miocene to Recent Sedimentary Dynamics of the Lower Niger Basin

The delta plain occupying the lower, ~200km, reach of the Niger River consists of up to 4km of continental sands comprising the Plio-Pleistocene Benin Formation (Whiteman 1982). Together with the underlying 2.8km Miocene sedimentary sequence of the Abgada Formation, these units reflect significant regional, extensional-driven subsidence (Cohen and McCay 1996). Altogether, the Pliocene to Quaternary history of the Niger River Basin is marked by substantial deltaic construction and floodplain aggradation caused by fluvial delivery of voluminous terrestrial sediments.

Global climatic oscillations in the Quaternary led to episodes in which the Niger River was temporarily severed from its deltaic outlet (*Goddard Earth Sciences Data and Information Services Center* URL: [www.daac.gsfc.nasa.gov](http://www.daac.gsfc.nasa.gov)). Geologically very recent wave action in the east equatorial Atlantic has eroded the morphology of the Late Pleistocene landscape reflected by present-day arrays of barrier bays, lagoons and long-shore spits (Sexton and Murdy 1994).

#### 5.5 Geophysical Observables: Free-Air Surface Gravity Anomalies

In the current study we find it instructive to utilize the additional constraint of crust-corrected surface gravity anomalies. This approach seeks to effectively remove the crustal isostatic contribution embedded in the observed free-air anomalies. The gravity anomalies are represented in terms of spherical harmonic expansion up to degree 128, corresponding to a minimum half-width of 155 km. Naturally, the amplitudes and range of crust-corrected free-air gravity are subdued relative to the original satellite derived measurements. The correction can include signals imparted by post-glacial rebound where applicable (e.g. North America). Furthermore, the crust-corrected approach has significantly improved the delineation of potential

internal mantle heterogeneities associated with mantle flow under Africa (Forte et al. 2010) and North America (Perry and Forte 2010).

Using an updated global model of crust-corrected surface gravity anomalies (A.M. Forte 2010, personal communication) that include predictions from 3-D convection simulations derived from joint seismic-geodynamic tomography models, we assess basin-scale surface gravity anomaly patterns for the Nile, Mississippi, Amazon, and Niger River systems (Fig. 5.2).

Inland portions of selected drainage basins show an overall pattern in which tributary rivers and higher-order streams converge about free-air gravity anomaly lows into main trunk rivers (see Fig 5.1 for major river network architecture). Furthermore, the gravity field shows significant negative values around continental margins increasing in amplitude towards the lower reaches of the Nile, Mississippi and Amazon Rivers.

Regarding the current study's treatment of extracting the relative contributions of crustal structure, flexure, and long-term fluvial processes in estimating anomalous neo-tectonic subsidence (ANTS', Chapter 4), patterns of crust-corrected free-air gravity anomalies about these basins are particularly interesting.

Gravity anomalies expressed on the short length scales (a few hundreds of kilometres) associated with the river basins studied here will be mainly sensitive to density anomalies in the upper-most mantle that generate flow below lithospheric depths. This is evident in the viscous flow response functions shown in Perry and Forte (2010). The high valued ANTS' and the negative gravity fields associated with the middle and lower reaches of the Nile and Mississippi drainage basins are certainly in agreement. A clear example is the exceptionally linear N-S course of the Egyptian Nile along the Northeast African gravity low. To a lesser extent, though not insignificant, both the course of the Arkansas River and the trend of the Gulf of Mexico rift (GMRM) lineament, to the south, correlate with the regional gravity low of central Texas into western Louisiana. The relationship between values of anomalous neo-tectonic subsidence and surface gravity anomalies for the Amazon and Niger basins is not as apparent. Additional geodynamic considerations are discussed later in this chapter.

We do not consider the observation that negative amplitudes of ANTS' and crust-corrected free-air gravity are found where rivers debouche into their respective ocean basins as coincidental. The flux of terrestrial sediment entrained in continental fluvial systems should, over late Cenozoic time-scales, flow towards regions of decreasing potential energy. Given that the ocean basins serve as the ultimate base level for exported terrestrial material, both the observed and crust-corrected gravity field may serve as geophysical proxies for studying the impact of mantle dynamics on the sediment routing system. If indeed the crust-corrected gravity field sufficiently reflects contributing forces from the convecting mantle, its predictions can be utilized to resolve past and ongoing dynamics of the continental clastic 'factory'. The notion that deep earth dynamics may exert some control upon geologically recent (i.e. neotectonic) surface processes not only remains plausible but gains momentum as related forthcoming studies will prove fruitful (e.g. TOPO-EUROPE, Cleoteigh et al. 2006; TOPO-Africa; Bishop 2007).

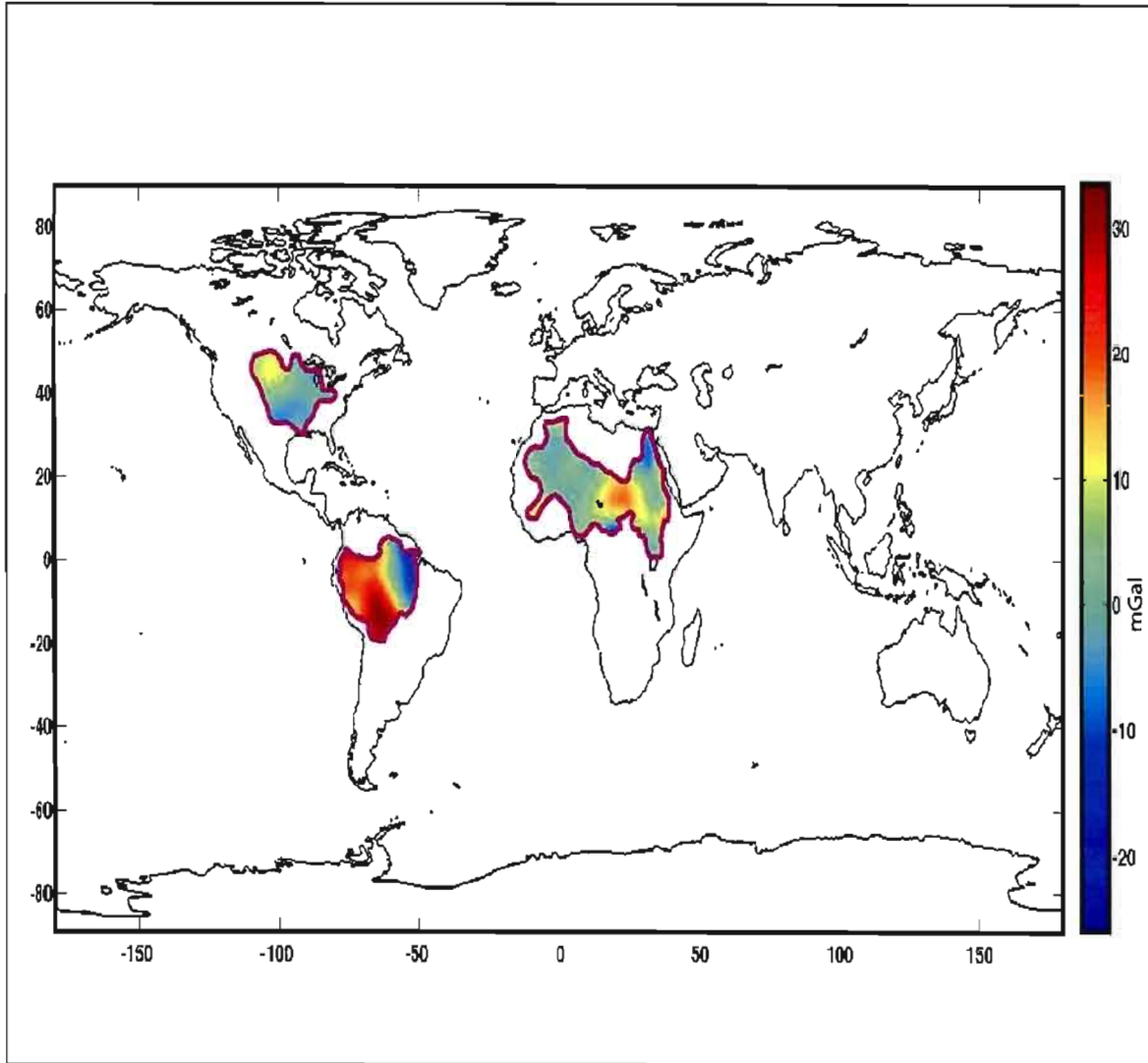


Figure 5.2 Crust-corrected free-air surface gravity anomalies (mGal) for selected basins concurrent to this study.

### 5.6 Seismic Tomography and Reconstructed Variations in Mantle Temperature

In lieu of various uncertainties regarding the analysis of surface gravity anomalies (Forte 2007 *and references therein*) we supplement gravity data and corrections with seismic tomography models in the attempt to detect signals imparted by dynamics occurring within the mantle (Capitanio et al. 2009; Forte et al. 2010).

Figure 5.3 shows four different radial cross-sections of reconstructed mantle temperature variations (Simmons et al. 2007) from the surface to core-mantle boundary of the regions pertinent to the current study. These maps are particularly useful to resolve mantle temperature heterogeneity at sub-continental scales and determine potential geodynamic sources originating in the mantle. Rendering a sound vision of mantle structure and kinematics will elucidate possible connections with geologically recent fluvial basin dynamics and configuration.

Shallow, anomalous cold mantle material residing below the Niger and Mississippi River systems is apparent. In close proximity to the shoreline deltaic plain and offshore delta, the lower reach of the Niger River is located above the coldest material in the region's underlying mantle. The negative-buoyancy associated with cold mantle may dictate some of the fluvial architecture and flux of clastic material (e.g. Mitrovica et al. 1989; Heller et al. 2003) out of Africa and into the Atlantic. Indeed, if such anomalously cold material causes time-dependent vertical motions about the Northwest African margin (Moucha et al. 2009), the structure and dynamics occurring in the mantle becomes an important candidate for processes associated with sea-level change (see *Section 5.1.4 for further details on the wave-dominated morphometry of the Niger Delta*).

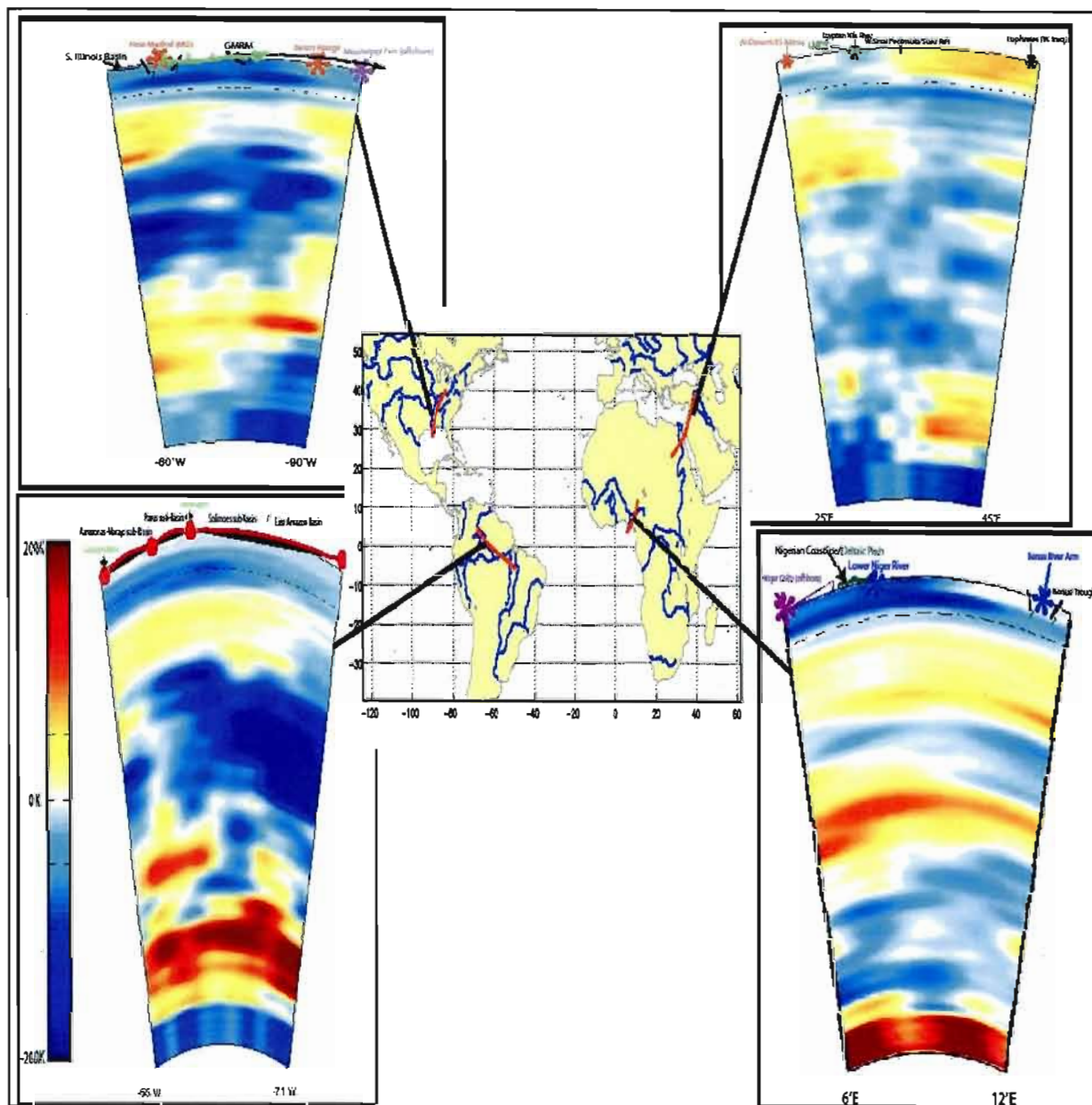


Figure 5.3 Radial cross-sections of reconstructed mantle temperature variations from the surface to core-mantle boundary for selected regions. Lower bounds of profiles is  $\sim 2800$ km depth. Red lines (arcs) in center map trace the surface geodetic paths of respective profiles. Profiles are derived from the joint seismic-geodynamic tomography model of Simmons et al. 2007. Temperature scale included in the Amazon profile (in Kelvin) can be applied to all cross-sections. Key features depicted in Fig 5.1 are marked for reference and follow the same map key/legend. Blue and purple asterisk denote the locales of major river channels/segments and offshore delta/fans, respectively. GMRM- Gulf of Mexico Rifted Margin. Drawn single and paired fault traces (grabens) are not to scale (vertical) as their depth extent/penetration is uncertain.

The source of the cold upper-mantle below the North American craton, including a good portion of the Mississippi Basin and environs, has been attributed to an exceptionally strong, Fe-Mg enriched deep-seated 'tectosphere' (Forte and Perry 2002). A large, relatively continuous body of cold material, too, occupies much of the mid-mantle in the region. Forte et al. (2007) attributed this relatively massive 'unit' to the descent of the ancient Farallon slab; a remnant vestige of late-Cretaceous Pacific ocean-crust. We propose that the pulling force, or downward suction, imparted by this large mantle body may impact the Mississippi fluvial Basin in a manner that both guides its tributary network and entrenches its main trunk River. Following this perspective, the significant aggradational fluvial landforms and  $\geq 100\text{m}$  of surface lowering since the Pliocene (Van Arsdale 2007) in the Mississippi Valley may be, in part, owed to forces originating in the mid-mantle. Additional sedimentological and geomorphological features with potential connections to mantle-related geodynamic processes include: (1) Sizeable terrestrial sediment sequences in the northern Gulf of Mexico (Appendix 1 and Section 5.2), (2) an engendered Mississippi Embayment/GMRM as long-wavelength, low-amplitude surface depressions and (3) the staying power of the lower Mississippi River course (Knox 2007).

At 200km - 300km mantle depths below the Purus and Amazonas-Marajo sub-Basins we observe relatively cold material and agree with previous studies that posit strong cratonic roots associated with the Proterozoic Central Brazilian and Guyana Shields (Perez-Guysseye et al. 2007). More striking, though, is the high negative amplitude temperature body extending from the East Amazon Basin (EAB) to the Purus sub-Basin in the middle to upper mantle, respectively. The free-air gravity pattern (Fig 5.2) about the Amazon Basin proper reveals the Nazca plate signature of shallow subduction in the west that increases dip and depth penetration towards the east. Recent studies have suggested this long-wavelength upwelled region, the so-called Fitzcarrald Arch, marking the western limit of the EAB is a result of the post-Miocene subduction of an aseismic spreading ridge embedded in the Nazca Plate (Espurt et al. 2007). If the long-wavelength positive surface feature is indeed associated with subduction dynamics, the confluence of major tributaries, such as the Purus and Negro Rivers, coupled with the drainage course of the main Amazon River channel could, in tandem, be guided by sub-lithospheric dynamics (Mitrovica et al. 1989).

The several hundred meters of anomalous neo-tectonic subsidence derived in this study, dip inflection of the leading edge of the Nazca plate and the concurrent shoaling of the mid-upper mantle negative thermal anomaly directly below the Purus sub-Basin indicates important geodynamics operating about the region. Based on the architecture and lithological characteristics of fluvial deposits, Costa et al. (2001) highlighted several drainage anomalies thought to have occurred since the Pliocene. These included periodic damming of main Amazon River channels, formation of local lacustrine depressions, abandoned meanders, and exceptionally straight fluvial segments. The authors attributed the sedimentary features and geomorphic processes to vertical crustal movement operating <1000km from the Atlantic Ocean. Similarly, other independent studies found evidence for voluminous sediment retention and initiation river-lakes acting as late-Pliocene regional depocenters in the Lower Amazon (Rodazz et al. 2006). Analogous to the Farallon slab dynamics occurring deep below North America, we propose that negative buoyancy associated with the leading edge of the Nazca Plate has, and continues to, impart sufficient energy to force vertical motions well into the upper-crust. The incipient effect on the evolution of the Amazon fluvial system and the impression in its sedimentary record can find partial resolve in the geologically recent coupling of surface processes, plate interaction, and internal mantle dynamics.

The reconstructed mantle temperature field below Northeast Africa and the Middle East is rather unique when compared to the other terrestrial basins discussed above. A subdued negative thermal anomaly in the mantle lithosphere is contained neatly below the trend of the Egyptian Nile. Although this low amplitude anomaly can be sinuously traced into the deeper mantle, we believe that the strong positive thermal anomaly associated with the spreading of the Red Sea (Vita-Finzi 2001; Daradich et al. 2003; Forte 2010) to the east and the mantle upwelling under the East African Rift system (Lithgow-Bertelloni and Silver and 1998; Nyblade et al. 2000; Simmons et al. 2006) to the south has created a prominent northwest tilted crust-lithosphere system within Egypt and Sudan. Operating under this mechanism, the persistent linear course of the Nile, along the Dongala-Salima suture, with sediment provenance and delivery from the highlands of Ethiopia (Pik et al. 2007) to the Sudd Basin, respectively, becomes readily explained. Our confidence in deep-earth convection, revealed here by one of the largest present-day mantle upwellings, exerting a primary control on drainage basin architecture is supported by

the current study's results of ANTS': The amplitude of subsidence rendered about the post-Miocene Egyptian Nile (Section 4.6) agrees with a systematic dynamic depression (see Fig 1.1) and regional tilt towards the Mediterranean Sea. As well, serving as a major intra-continental depocenter for sediments delivered by the Blue Nile, the calculated anomalous subsidence around central Sudan (Sudd) provides support to processes operating outside the crust-lithosphere system.

Though the current study does not explicitly explore time-dependent flow patterns of mantle convection, 'corner-flow' associated with the cooling of transient hot mantle material is observed in many tectonic settings (e.g. mantle wedge within subduction systems (Burgess et al. 2001; Gerya 2007), within the lithosphere during basin inversion (Issler et al. 1989), and plutonic emplacement (Brown 2008)). Pertinent to the geodynamic setting of East Africa, we use the time-dependent modeled dynamics of rising anomalously warm mantle material, since the Neogene, below the Colorado Plateau as a fitting example (*see* Figure 1 (a-f) *in* Moucha et al. 2008; Figure 1(a,b) *in* Moucha et al. 2009). These studies have demonstrated the likelihood of a mantle source behind rapid surface uplift and the region's 'excessive' elevation. The authors show that the settling of a warm buoyant mantle body during cooling is accompanied by counter rotation at its peripheries; and, aptly call the process 'corner-flow'. Upon sufficient cooling, then, the peripheral material acquires negative buoyancy so as to initiate descent. In this way, then, greater Nile Basin can serve as a quasi-archetype model for a fluvial system intimately tied to mantle convection dynamics. Two broad scale geomorphic features elucidate this suggestion: (1) The radial pattern of tributary rivers feeding the Blue Nile in the Lake Tana region (Gani et al. 2007) is a well understood signature associated with drainage patterns above mantle upwellings (e.g. Burke and Wells 1989; Talbot and Williams 2009; Moore et al. 2009). (2) The middle and lower reaches of the Nile is flanked remarkably close to the limits of the Red Sea/East-African Rifts, making 'corner-flow' descent in the mantle a viable hypothesis to explain the fluvial architecture unique to the region.

## Conclusions

### 6.1 Motivation

While we feel our analysis of active fluvial basins is rather novel, the thorough review of assimilated data sets and previously generated models (see Chapter 2) referred to in the present study highlights the fact that our model is a scaffold constructed on the insightful work of numerous research teams. By employing a multi-tiered approach to resolve and marry current ideas of continent-scale geodynamics to basin-wide surface processes, we understand a liberal inclusion of diverse data sets in conjunction with assumptions made about relevant time and spatial scales can be somewhat precarious. In the following we conclude with a brief discussion of the methods I have employed, in particular their shortcomings, and the principal conclusion emanating from this study. I also wish to highlight potential improvements in methodology with a view to establishing a road map for future studies.

### 6.2 Importance of Crustal Model CRUST2.0

The preliminary steps in quantifying anomalous neo-tectonic subsidence are heavily reliant on the crustal structure, particularly the sediment distribution, revealed in CRUST2.0. The sediments in this crustal model are assumed to have constant density and this of course ignores the effect of porosity change with depth due to increasing pressure. The effect of such pressure-induced changes in sediment density can be important in calculating the resulting isostatic-flexural response of the crust (e.g. Sykes 1996). Furthermore, the spatial resolution of the sedimentary structure in CRUST2.0 is too coarse to provide sufficiently detailed description of local changes in sediment structure on the scale of river basins we have studied. So long as regional crustal models increase in both resolution and accuracy, their ensuing inclusion in global compilations will no doubt advance our understanding of the architecture and physical properties related to the earth's crust.

### 6.3 Isostatic and Flexural Assumptions

One of the challenges faced in the current study is how to properly treat the behavior of the crust in terms of flexural deformation. At characteristic wavelengths of large terrestrial basins, there exists a lacking consensus as to the dominant behavior (e.g. hydro-isostatic, elastic or visco-elastic) that most accurately expresses the response of the earth's outer-surface and underlying crust to surface load variations. Our attempt to include both hydro-isostatic and elastic flexural mechanisms required the assumption that fluvial erosion and deposition causes deflections of the earth's surface at intrabasinal scales. On the other hand, continent and basin-wide vertical configurations were analyzed using the principles of 'simple' hydro-isostasy such that the long-term (i.e. fluid) limit of crustal equilibrium was achieved; specifically, through the normalization with respect to reference column and underlying medium. The amplitudes of erosion-induced isostatic rebound were formulated in a parallel manner, but assuming an elastic-flexural loading model for the crust-lithosphere system.

The information in Table 4.1 contains the relevant values and parameters used to analyze the flexural response of post-Miocene fluvial dynamics for the selected terrestrial basins and their ocean-bound drainage network. There is no denying that assumptions abound regarding: (1) the elastic thickness of the lithosphere and its equivalent effective rigidity as well as (2) the sediment thicknesses along the lower reaches of each major river channel. With respect to the latter, our choice to chart out sedimentary sequences and lithostratigraphic markers contained within them stems from our goal to establish whether erosion or deposition has dominated specific locales.

The 2-D elastic-flexure approximation is admittedly simple and likely over-estimates (e.g. Driscoll and Karner 1994) the amplitudes of anomalous elevations. However we feel the kinematic model, in the form of a moving rectangular load, captures what we envision to be a traveling 'front' along the longitudinal axis of active fluvial systems. This perspective differs from conventional basin analysis in which the geometry is rendered transverse to the main

incising river. The latter approach tends to portray the archetypal basin architecture in a form analogous to a 'steerhorn'. This particular 'saucer-like' geometry is certainly befitting to illustrate the interim transport of sediments from, say, elevated terrain to a basin's main artery; for example, delimiting source lithologies in regional stratigraphic sequences embedded in alluvial fans and strath terraces.

#### 6.4 Simplified Fluvial Modeling

Our depiction of fluvial systems reflects the tendency for material, over sufficient time scales, to emerge from a terrestrial basin into the marine environment. Though rudimentary and incomplete in simulating the inherent complexity of sedimentary dynamics, implementing only one of two possible conditions at a given segment facilitated the reduction of surface processes into a 2-D realm. Upon sound interpretation of site-specific sedimentary field studies we are able to effect a sort of model 'front' that will either unload or add material to a given fluvial segment; essentially simulating denudation and intrabasin deposition, respectively.

Though modeling different elastic thicknesses is indeed imperative, our simplification emanates from the fact that effective lithospheric rigidity varies in both space and time. Regarding the former domain, the transects that delineate each river segment as they approach marine outlets tend to cross tectonic provinces typified by their respective age, lithology, and characteristic erodibility. Site-specific studies accounting for processes inherent in both short and long-range transport dynamics would certainly capture local geomorphic variability to a greater extent than those garnered in this study.

#### 6.5 Time-Dependent Rheology

We also acknowledge the well-established notion that elastic thickness, as well as crustal thickness, changes at geological time-scales greater than  $10^5$  years (Watts 2001). However, it is beyond the scope of this study to ascertain the portion of the crust that changes its rheological properties over time. Even focusing solely on the overland flux of material by assuming all thickness change commences in the near-surface environment would require at least detailed 3-D

renderings of crustal structure and the corresponding strain imparted by changes in lithostatic pressure. Given the rapid advances in computational power and efficiency (e.g. Li et al. 2004), we are positive and confident that such facets of crustal deformation will become increasingly resolved.

## 6.6 Concluding Comments and Perspectives

Our logic began from the observation that present-day active drainage basins are associated with significant amplitudes of negative dynamic and non-isostatic topography predicted by mantle convection and crustal models, respectively. We then sought additional constraints to resolve striking correlations between the history and on-going dynamics of certain large fluvial basins and crustal to sub-crustal geophysical phenomena currently associated with these regions.

Global seismic tomographic models are formulated in terms of elastic-wave properties of the mantle, so travel-time analysis and proper seismic velocity-to-density conversions are paramount to rendering the internal structure of the earth (Simmons et al. 2009). Though there is no unified vision about how to convert the raw data from teleseismic studies to equivalent density temperature fields, important constraints invoked over the last 15 years have greatly improved the accuracy and resolution of tomographic models (Simmons et al. 2010). Continuing refinements of additional parameters regarding mineral physical and thermo-chemical properties the mantle will increase our understanding of radial and lateral heterogeneities in the deep earth.

The process of mantle convection likely extended far back in geological time, perhaps as early as the beginning of the Archean (Bercovici et al. 2000). The early earth, though, was certainly different from the one we know today. Correlating the slow cadence of mantle convection, however intuitive, to simply the prominent large-scale surface geological structures have become, nowadays, accepted as conventional wisdom. With the perspective of the current understanding and ongoing efforts towards accurate renderings of earth structure as a whole, the current study's overall goal of merging deep-seated geodynamics with the countenance of geologically recent fluvial basin processes and architecture is a new, and in our view, bold proposition. The connections proposed in this study exemplify the fact that the study of

geological processes must become increasingly multi-disciplinary and the future work should continue to strive to present the evolving earth in terms of a finely balanced integrated system with complex feedbacks between the surface and the deep interior.

## REFERENCES

- Abdelsalam, M.G. AND R.J. Stern. 1996. Sutures and shear zones in the Arabian-Nubian Shield. *Journal of African Earth Sciences*, Volume 23, Issue 3, DOI: 10.1016/S0899-5362(97)00003-1.
- Abu El-Ella, R. 2007. The neogene-Quaternary section of the Nile Delta: Geology and hydrocarbon potential. *Journal of Petroleum Geology*, Volume 13 Issue 3, Pages 329 – 340
- Albritton, C., Brooks, J.E., Issawi, B. and Ahmed Swedan. 1990. Origin of the Qattara Depression, Egypt. *Geological Society of America Bulletin*. 102(7): pp.952-960
- Allen, P.A., Allen, J.R., 2005. Basin Analysis: Principles and Applications, 2nd Edition. Am. Blackwell Publishing, Incorporated, Oxford, United Kingdom.
- Artemieva, I. M., and W. D. Mooney (2001), Thermal thickness and evolution of Precambrian lithosphere: A global study, *J. Geophys. Res.*, 106, 16,387–16,414, doi:10.1029/2000JB900439.
- Bercovici, D. , Ricard, Y. and Mark A. Richards. 2000. The Relation Between Mantle Dynamics and Plate Tectonics: A Primer. *The History and Dynamics of Global Plate Motions*, GEOPHYSICAL MONOGRAPH 121, M. Richards, R. Gordon and R. van der Hilst, eds. American Geophysical Union, pp5–46.
- Bird, P. [1995] Lithosphere dynamics and continental deformation , *Rev. Geophys.*, Supplement: U.S. National Report to IUGG 1991-94, 379-383.
- Bishop, P. 2007. Long-term landscape evolution: linking tectonics and surface processes. *Earth Surface Processes and Landforms*; v.32; ISSN 3, pp. 329-365
- Blum, M., Michael D., Tomkin, Jonathan H., Purcell, Anthony, Lancaster, Robin R. 2008. Ups and downs of the Mississippi Delta. *Geology* 36: 675-678
- Braitenberg, C. and J. Ebbing. 2009. The GRACE-satellite gravity field in analysing large scale, cratonic or intracratonic basins. *Geophysical Prospecting*, 57, 559-571. doi: 10.1111/j.1365-2478.2009.00793. x 10)
- Brown, M. 2007. Crustal melting and melt extraction, ascent and emplacement in orogens: mechanisms and consequences. *Journal of the Geological Society* v. 164; no. 4; p. 709-730.
- Burbank, D. W. and Anderson, R. S. (2000) *Tectonic Geomorphology*. Blackwell Science, 274 pp.
- Burgess and Moresi. 1999 .Modelling rates and distribution of subsidence due to dynamic topography over subducting slabs: is it possible to identify dynamic topography from ancient strata? . *Basin Research* ;v.11 no. 4; p.305-314

- Burgess, P. M., Gurnis, M., and Moresi, L., 1997. Formation of sequences in the cratonic interior of North America by interaction between mantle, eustatic and stratigraphic processes, *Bulletin of the Geological Society of America* 108, 1515-1535, 1997.
- Burgess, P.M., Gurnis, M., 1995. Mechanisms for the formation of cratonic stratigraphic sequences. *Earth Planet. Sci. Lett.* 136, 647–663.
- Burke, K. and Gordon L. Wells. 1989. Trans-African drainage system of the Sahara: Was it the Nile? *Geology*; v. 17; no. 8; p. 743-747; DOI: 10.1130/0091-7613(1989)017<0743:TADSOT>2.3.CO;2
- Capitanio, F.A. , Faccenna, C. and R. Funiciello. 2009. The opening of Sirte basin: Result of slab avalanching?. *Earth and Planetary Science Letters*, Volume 285, Issues 1-2, Pages 210-216, ISSN 0012-821X, DOI: 10.1016/j.epsl.2009.06.019.
- Cardozo, N., Jordan, T., 2001. Causes of spatially variable tectonic subsidence in the Miocene Bermejo foreland basin. Argentina, *Journal of Basin Research* 13, 335–357.
- Castro, A. Gerya, T.V. (2007) Magmatic implications of mantle wedge plumes: Experimental study. *Lithos*, 103, 138-148.
- Chase, C.G. A.J. Sussman, and D.D. Coblenz . 2009. Curved Andes: Geoid, forebulge, and flexure. *Lithosphere* v. 1, p. 358-363, doi:10.1130/L67.1
- Champagnac, J. D., Molnar, P., Anderson, R. S., Sue, C. Delacou, B. 2007. Quaternary erosion-induced isostatic rebound in the western Alps. *Geology*, vol. 35, Issue 3, p.195. DOI:10.1130/G23053A.1
- Christensen, N. I., and W. D. Mooney (1995), Seismic velocity structure and composition of the continental crust: A global view, *J. Geophys. Res.*, 100(B6), 9761–9788, doi:10.1029/95JB00259
- Cloetingh, S.A.P.L., P.A. Ziegler, P.J.F. Bogaard, P.A.M. Andriessen, I.M. Artemieva, G. Bada, R.T. van Balen, F. Beekman, Z. Ben-Avraham, J.-P. Brun, H.P. Bunge, E.B. Burov, R. Carbonell, C. Facenna, A. Friedrich, J. Gallart, A.G. Green, O. Heidbach, A.G. Jones, L. Matenco, J. Mosar, O. Oncken, C. Pascal, G. Peters, S. Sliupa, A. Soesoo, W. Spakman, R.A. Stephenson, H. Thybo, T. Torsvik, G. de Vicente, F. Wenzel, M.J.R. Wortel and TOPO-EUROPE Working Group. 2007. TOPO-EUROPE: The geoscience of coupled deep Earth-surface processes, *Global and Planetary Change*, Volume 58, Issues 1-4, TOPO-EUROPE: the Geoscience of Coupled Deep Earth-Surface Processes, July Pages 1-118, ISSN 0921-8181, DOI: 10.1016/j.gloplacha.2007.02.008.
- Cohen H.A and Ken McClay. 1996. Sedimentation and shale tectonics of the northwestern Niger Delta front. *Marine and Petroleum Geology*, Volume 13, Issue 3, Pages 313-328. DOI: 10.1016/0264-8172(95)00067-4.

Costa, J.B.S., Lea Bemerguy R., Hasui Y.; M. da Silva Borges. 2001. Tectonics and paleogeography along the Amazon river. *Journal of South American Earth Sciences*, Volume 14, Issue 4, pp. 335-347. DOI: 10.1016/S0895-9811(01)00025-6.

Crouch, R.W. 1959. Inspissation of post-Oligocene sediments in southern Louisiana. *Geological Society of America Bulletin* 70(10): p.1283-1292

Crosby, A. G., S. Fishwick, , and N. White. 2010. Structure and Evolution of the Intracratonic Congo Basin. *GEOCHEMISTRY, GEOPHYSICS, GEOSYSTEMS, VOL. ???, XXXX*, DOI:10.1029/

D'Agostino , J. A. Jackson ,F. Dramis ,R. Funicello. 2001. Interactions between mantle upwelling, drainage evolution and&nbsp;active normal faulting: an example from the central Apennines(Italy). *Geophysical Journal International*; v.147 ,No. 2 , p: 475-497 DOI: 10.1046/j.1365-246X.2001.00539.x

Daradich, A., J. X. Mitrovica and R. N. Pysklywec. 2002.Mantle flow modeling of the anomalous subsidence of the Silurian Baltic Basin. *Geophys. Res. Lett.*, 29(6), 4399-4402.

Daradich, A., Mitrovica, J.X., Pysklywec, R.N., Willett, S.D., Forte, A.M.,. 2003. Mantle flow, dynamic topography, and rift-flank uplift of Arabia, *Geology*, 31 (10), 901-904.

Downey, N. and M. Gurnis (2009), Instantaneous dynamics of the cratonic Congo Basin,

Driscoll, N.W. and G.D. Karner (1994). Flexural deformation due to Amazon Fan loading: A feedback mechanism affecting sediment delivery to margins. *Geology*, v. 22: 1015-1018.

Einsele, Gerhard. 2000. *Sedimentary Basins: Evolution, Facies, and Sediment Budget* 2nd ed., XII, 792p.

El Bastawesy,M., Faïd, A. and El Sayed El Gamma. 2010. The Quaternary development of tributary channels to the Nile River at Kom Ombo area, Eastern Desert of Egypt, and their implication for groundwater resources. *Hydrological Processes*, vol.24, no.13; pp.1856-1865.DOI: 10.1002/hyp.7623

ETOPO2v2 <http://www.ngdc.noaa.gov/mgg/fliers/01magg04.html>

Faccenna, C., F. Rossetti, TW Becker, S. Danesi, 37 and A. Morelli. (2008), Recent extension driven by mantle 38 upwelling beneath the Admiralty Mountains (East Antarctica). *Tectonics*. doi:10.1029/2007TC002197. 41

Figueiredo, J., C. Hoorn, P., van der Ven and E. Soares. 2009. Late Miocene onset of the Amazon River and the Amazon deep-sea fan: Evidence from the Foz do Amazonas Basin. *Geology*; July 2009; v. 37; no. 7; p. 619-622; DOI: 10.1130/G25567A.1

Flesch, L., Corne Kreemer .2009. Gravitational potential energy and regional stress and strain rate fields for continental plateaus: Examples from the central Andes and Colorado Plateau, *Tectonophysics*, Volume 482, Issues 1-4, DOI: 10.1016/j.tecto.2009.07.014.

Forte, A.M., Mitrovica, J.X., Moucha, R., Simmons, N.A., Grand, S.P., 2007. Descent of the ancient Farallon slab drives localized mantle flow below the New Madrid seismic zone, *Geophys. Res. Lett.*, 34, L04308, doi:10.1029/2006GL027895

Forte, A.M., Quere, S., Moucha, R., Simmons, N.A., Grand, S.P, Mitrovica, J.X. and D.B. Rowley.2010. Joint seismic-geodynamic-mineral physical modelling of African geodynamics: A reconciliation of deep-mantle convection with surface geophysical constraints. *Earth and Planetary Science Letters*, Volume 295, Issues 3-4, 1 July 2010, Pages 329-341, ISSN 0012-821X, DOI: 10.1016/j.epsl.2010.03.017.

Forte, A.M., Moucha, R., Rowley, D.B., Quéré, S., Mitrovica, J.X., Simmons, N.A., Grand, S.P., 2009. Recent tectonic plate decelerations driven by mantle convection, *Geophys. Res. Lett.*, 36, L23301,

Forte, A.M., Perry, H.K.C., 2000. Geodynamic Evidence for a Chemically Depleted Continental Tectosphere, *Science*, 290 (5498), 1940–1944.

Forte, A.M, Peltier, W.R, Dziewonski, A.M and R.L.Woodward. 1993. Dynamic surface topography—a new interpretation based upon mantle flow models derived from seismic tomography. *Geophys. Res. Lett.* 19, 1555–1558

Frailley, C.D., Lavina, E.L., Rancy, A. and P. de Souza. 1988. A proposed Pleistocene/Holocene lake in the Amazon basin and its significance to Amazonian geology and biogeography. *Acta Amazonica*. vol. 18, no3-4, pp. 119-143

Gargani, J., Rigollet, C. and Sonia Scarselli.2010.Isostatic response and geomorphological evolution of the Nile valley during theMessinian salinity crisis. *Bull. Soc. géol. Fr.*, 2010, t. 181, no 1, pp. 19-26

Garzanti, E., Andò, S., Vezzoli, G., Abdel M.A., El Kammar, A. 2006. Petrology of Nile River sands (Ethiopia and Sudan): Sediment budgets and erosion patterns. *Earth and Planetary Science Letters*, Volume 252, Issue 3-4, p. 327-341.

Ghosh, Attreyee | Holt, William E | Flesch, Lucy M | Haines, A John .2006. Gravitational potential energy of the Tibetan Plateau and the forces driving the Indian plate. *Geology*. Vol. 34, no. 5, pp. 321-324.

Global Runoff Data Center

[http://www.bafg.de/cln\\_016/nn\\_266934/GRDC/EN/Home/homepage\\_\\_node.html](http://www.bafg.de/cln_016/nn_266934/GRDC/EN/Home/homepage__node.html)

Goddard Earth Science Data and Information Services Center (GES).

<http://www.daac.gsfc.nasa.gov>

- Govers, R. Paul Meijer, Wout Krijgsman. 2009. Regional isostatic response to Messinian Salinity Crisis events, *Tectonophysics*, Volume 463, Issues 1-4, p.109-129, DOI: 10.1016/j.tecto.2008.09.026.
- Graham, S., J. Famiglietti, and D. Maidment (1999), Five-Minute, 1/2°, and 1° Data Sets of Continental Watersheds and River Networks for Use in Regional and Global Hydrologic and Climate System Modeling Studies, *Water Resour. Res.*, 35(2), 583-587.
- Grand, S.P., van der Hilst, R.D. & Widiyantoro, S., 1997. Global seismic tomography: a snapshot of convection in the Earth, *GSA Today*, 7, 1–7.
- Gurnis, M., 1990. Bounds on global dynamic topography from Phanerozoic flooding of continental platforms. *Nature* 344, 754–756.
- Harry, D.L. and J. Londono. 2004. Structure and evolution of the central Gulf of Mexico continental margin and coastal plain, southeast United States. *Geological Society of America Bulletin*, 116; pp. 188-199. doi: 10.1130/B25237.1
- Hartley, R.W., Allen, P.A., 1994. Interior cratonic basins of Africa: relation to continental break-up and the role of mantle convection. *Basin Res.* 6, 65–113.
- Hay, W.H. 1998. Detrital sediment fluxes from continents to oceans. *Chemical Geology*, Volume 145, Issues 3-4, Pages 287-323
- Heine, C., Müller, R.D., Steinberger, B. and Torsvik, T., 2008, Anomalous subsidence in intracontinental basins, *Physics of the Earth and Planetary Interiors*, Special Volume on Computational Geology and Geodynamics, edited by B.J.P. Kaus, T.V. Gerya and D.W. Schmid, 171, 252-264
- Heller, P.L., Dueker, K., and McMillan, M.E., 2003, Post-Paleozoic Alluvial Gravel Transport as evidence of continental tilting in the U.S. Cordillera, *Geological Society of America Bulletin*, v. 115, no. 9, p. 1122-1132.
- Hospers, J. 1965. Gravity field and structure of the Niger delta, Nigeria, west Africa. *Geological Society of America Bulletin* 76(4): p.407-422
- Iaffaldano, G., H.-P. Bunge, and T. H. Dixon (2006), Feedback between mountain belt growth and plate convergence, *Geology*, 34, 893– 89.
- Issler, D. Herbert McQueen, H. and Christopher Beaumont. 1989. Thermal and isostatic consequences of simple shear extension of the continental lithosphere, *Earth and Planetary Science Letters*, Volume 91, Issues 3-4, Pages 341-358, ISSN 0012-821X, DOI: 10.1016/0012-821X(89)90008-3.

- Jadamec, .M.A. , Donald L. Turcotte, Peter Howell,. 2007. Analytic models for orogenic collapse, *Tectonophysics*, Volume 435, Issues 1-4, 1 Pages 1-12, DOI: 10.1016/j.tecto.2007.01.007.
- Jordan, T.E. .1981. Thrust loads and foreland basin evolution, Cretaceous, western United States. *Am. Assoc. Petrol. Geol. Bull.*, 65, 2506-2520.
- Kaban, M., Peter Schwintzer, Irina M. Artemieva, Walter D. Mooney. 2003. Density of the continental roots: compositional and thermal contributions, *Earth and Planetary Science Letters*, Volume 209, Issues 1-2Pages 53-69, DOI: 10.1016/S0012-821X(03)00072-4
- Karner, G.D. Neal W. Driscoll. 1999. Tectonic and stratigraphic development of the West African and eastern Brazilian Margins: insights from quantitative basin modelling *Geological Society, London, Special Publications*; v. 153; p. 11-40; DOI: 10.1144/GSL.SP.1999.153.01.02
- Knox, J.C. 2007. The Mississippi River system. In *Large Rivers: Geomorphology and Management* ,ed. Avijit Gupta, Ch.9 pp.145-177
- Laske, G., 2004. A New Global Crustal Model at 2 °— 2Degrees. URL: <http://mahi.ucsd.edu/Gabi/rem.dir/crust/crust2.html>.
- Laske, G., Masters, G., 1997. A global digital map of sediment thickness. *EOS Trans.*
- Leeder, M.R., .1991. Denudation, vertical crustal movements and sedimentary basin infill. *Geologische Rundschau* ;Volume 80 Issue - 2, p. 441- 458. DOI - 10.1007/BF01829376
- Lemoine, F.G., Kenyon, S.C., Factor, J.K.,|Trimmer, R.G., Pavlis, N.K, Chinn, D.S, Cox, C.M., Klosko, S.M., Luthcke, S.B., Torrence, M.H., Wang, Y.M., Williamson, R.G ,. Pavlis, E.C. and R.H. 1998. The Development of the Joint NASA GSFC and the National Imagery and Mapping Agency (NIMA) Geopotential Model EGM96. NASA pub. no. 19980218814 1.60:206861
- Li,F., Dyt, C. and Cedric Griffiths. 2004. 3D modelling of flexural isostatic deformation, *Computers & Geosciences*, Volume 30, Issues 9-10, Pages 1105-1115, ISSN 0098-3004, DOI: 10.1016/j.cageo.2004.08.005.
- Lithgow-Bertelloni, C., and J. H. Guynn (2004), Origin of the lithospheric stress field, *J. Geophys. Res.*, 109, B01408, doi:10.1029/2003JB002467
- Liu, S., and D. Nummedal. 2004.Late Cretaceous subsidence in Wyoming: Quantifying the dynamic component .*Geology* 2004 32: 397-400
- Lock, J. Harvey Kelsey, Kevin Furlong, and Adam Woolace. 2006. Late Neogene and Quaternary landscape evolution of the northern California Coast Ranges: Evidence for Mendocino triple junction tectonics. *Geological Society of America Bulletin*; 118: 1232 - 1246.

Loget N. and J. Van Den Driessche. 2006. On the origin of the strait of Gibraltar. *Sediment. Geol.*, 188-189, 341-356.

Mahmoudi, Ahmed El and Amir Gabr. 2009. Geophysical surveys to investigate the relation between the Quaternary Nile channels and the Messinian Nile canyon at East Nile Delta, Egypt. *Arabian Journal of Geosciences*. Vol. 2, no. 1, pp. 53-67.

Manglik et al. 2008. Finite element modelling of elastic intraplate stresses due to heterogeneities in crustal density and mechanical properties for the Jabalpur earthquake region, central India. *Journal of Earth System Science*; v. 117, p.103-111. DOI - 10.1007/s12040-008-0001-6

McKenzie, D.P., 1978. Some remarks on the development of sedimentary basins. *Earth Planet. Sci. Lett.* 40, 25–32.

McQuarrie, N., and D. W. Rodgers .1998. Subsidence of a volcanic basin by flexure and lower crustal flow: The eastern Snake River Plain, Idaho. *Tectonics*, 17(2), 203–220, doi:10.1029/97TC03762.

Mertes, L.A.K. and Thomas Dunne. 2007. Effects of tectonism, climate change, and sea-level change on the form and behaviour of the modern Amazon River and its Floodplain. In *Large Rivers: Geomorphology and Management* ed. Avijit Gupta, Ch.8 pp.115-140

Miall A. D . 2006. How do we identify big rivers?: And how big is big?. *SEDIMENTARY GEOLOGY*, 186:39–50.

Milliman, John D.; Syvitski, James P. M.1992. Geomorphic/Tectonic Control of Sediment Discharge to the Ocean: The Importance of Small Mountainous Rivers .*The Journal of Geology*, vol. 100, issue 5, pp. 525-544.

Mitrovica, J. X., C. Beaumont, and G. T. Jarvis (1989), TILTING OF CONTINENTAL INTERIORS BY THE DYNAMICAL EFFECTS OF SUBDUCTION, *Tectonics*, 8(5), 1079–1094, doi:10.1029/TC008i005p01079.

Mooney, W. D., G. Laske, and T. G. Masters (1998), CRUST 5.1: A global crustal model at 5° • 5°, *J. Geophys. Res.*, 103(B1), 727–747, doi:10.1029/97JB02122.

Mooney, W.D., Vidale, J.E., 2003. Thermal and chemical variations in subcrustal cratonic lithosphere: evidence from crustal isostasy. *Lithos* 71 (2–4), 185–193.

Moucha, R., Forte, A.M., Mitrovica, J.X., Rowley, D.B., Quéré, S., Simmons, N.A., Grand, S.P., 2008. Dynamic Topography and Long-Term Sea-Level Variations: There Is No Such Thing as a Stable Continental Platform, *Earth and Planetary Science Letters*, 271(1-4), 101-108.

Moucha, R., Forte, A.M., Rowley, D.B., Mitrovica, J.X., Simmons, N.A., Grand, S.P., 2009. Deep mantle forces and the uplift of the Colorado Plateau, *Geophys. Res. Lett.*, 36, L19310, doi:10.1029/2009GL039778.

- Moucha, R., Forte, A.M., Rowley, D.B., Mitrovica, J.X., Simmons, N.A., Grand, S.P., 2008. Mantle convection and the recent evolution of the Colorado Plateau and the Rio Grande Rift valley, *Geology*, 36(6), 439-442.
- Nyblade, A A. Owens, T.J.; Gurrola, H. Ritsema, J. and C.A Langston. 2000. Seismic evidence for a deep upper mantle thermal anomaly beneath east Africa. *Geology*, vol. 28, Issue 7, p.599
- Pari, G. and W.R. Peltier. (2000) Subcontinental mantle dynamics: A further analysis based on the joint constraints of dynamic surface topography and free-air gravity. *GRL*; VOL 105; PART B3, pages 5635-5662
- Pari, G., 2001. Crust 5.1-based inference of the Earth's dynamic surface topography: geodynamic implications, *Geophys. J. Int.* 144, 501–516.
- Pazzaglia, F., and T. Gardner (1994), Late Cenozoic flexural deformation of the middle U. S. Atlantic passive margin, *J. Geophys. Res.*, 99(B6), 12143-12157.
- Peizhen, Z., P. Molnar, and W. R. Downs. 2001. Increased sedimentation rates and grain sizes 2–4 Myr ago due to the influence of climate change on erosion rates. *Nature*; 410, 891-897
- Perez-Gussinye, M. and Watts, A. B. 2005 .The long-term strength of Europe and its implications for plate-forming processes .*Nature* ;V 436,p. 381 - 384
- Pérez-Gussinyé, M., A. R. Lowry, and A. B. Watts (2007), Effective elastic thickness of South America and its implications for intracontinental deformation, *Geochem. Geophys. Geosyst.*, 8, Q05009, doi:10.1029/2006GC001511.
- Perry, H.K.C., Eaton, D.W.S., Forte, A.M., 2002. LITH5.0: A revised crustal model for Canada based on LITHOPROBE results, *Geophys. J. Int.*, 150 (1), 285-294.
- Perry, H.K.C., Forte, A.M., Eaton, D.W.S., 2003. Upper-mantle thermochemical structure below North America from seismic-geodynamic flow models, *Geophys. J. Int.*, 154 (2), 279– 299.
- Perry, H. K.C. and A.M. Forte. 2010. Upper mantle thermochemical structure from seismic-geodynamic flow models: constraints from the Lithoprobe initiative. *Canadian Journal of Earth Sciences*, Vol.47, no.4, , pp. 463-484(22)
- Phillips, F.M., John P Ayarbe, J.Bruce J Harrison, David Elmore. 2003. Dating rupture events on alluvial fault scarps using cosmogenic nuclides and scarp morphology. *Earth and Planetary Science Letters*, Volume 215, Issues 1-2, 15 Pages 203-218, DOI: 10.1016/S0012-821X(03)00419-9.
- Pik, R., Marty, B. Carignan and J Lavé. 2003. Stability of the Upper Nile drainage network (Ethiopia) deduced from (U-Th)/He thermochronometry: implications for uplift and erosion of the Afar plume dome. *Earth and Planetary Science Letters*, 215, 73–88.

Pollard, D. and Raymond C. Fletcher. *Fundamentals of Structural Geology* . 512 pages. Cambridge University Press

Potter, P.E., 1978. Significance and origin of big rivers. *Journal of Geology* 86, 13–33.

Prezzi, C., Cornelius E. Uba, Hans-Jurgen Gotze. 2009. Flexural isostasy in the Bolivian Andes: Chaco foreland basin development, *Tectonophysics*, Volume 474, Issues 3-4, 10 Pages 526-543, DOI: 10.1016/j.tecto.2009.04.037.

Pysklywec, R., and J.X. Mitrovica, 1999. The Role of Subduction-Induced Subsidence in the Evolution of the Karoo Basin, *J. Geology*, 107, 155-164.

Pysklywec, R., and J.X. Mitrovica, 2000. Mantle Flow Mechanisms of Epeirogeny and Their Possible Role in the Evolution of the Western Canada Sedimentary Basin, *Can. J. Earth Sci.*, 37, 1535-1548.

Ranalli, G. 200 Rheology of the crust and its role in tectonic reactivation, *Journal of Geodynamics*, Volume 30, Pages 3-15, DOI: 10.1016/S0264-3707(99)00024-1.

Roddaz, M., Brusset, S., Baby, P. and Gerard Herail. 2006. Miocene tidal-influenced sedimentation to continental Pliocene sedimentation in the forebulge-backbulge depozones of the Beni-Mamore foreland Basin (northern Bolivia). *Journal of South American Earth Sciences*, Volume 20, Issue 4, Pages 351-368, ISSN 0895-9811, DOI: 10.1016/

Rodger, M. and Watts, A. B. and Greenroyd, C. and Peirce, C. and Hobbs, R. W. 2006. 'Evidence for unusually thin oceanic crust and strong mantle beneath the Amazon fan. *Geology*., 34 (12). pp. 1081-1084.

Ryan, W.B.F. 1978. Messinian badlands on the southeastern margin of the Mediterranean Sea. *Marine Geology*, Volume 27, Issues 3-4; pp 349-363, Messinian erosional surfaces in the Mediterranean ISSN 0025-3227, DOI: 10.1016/0025-3227(78)90039-7.

Said, R., 1981. *The Geological Evolution of the River Nile*. New York: Springer, 151p.

Scholz, C.H. 2002. *The mechanics of earthquakes and faulting*. Cambridge University Press; 471 pp.

Slater, J. G. and P. A. F. Christie. 1980. Continental stretching: An explanation of the post-Mid Cretaceous subsidence of the Central North Sea Basin, *J. Geophys. Res.*, 85, 3711-3739.

Seber et al. 2001. Crustal model for the Middle East and North Africa region - Implications for the isostatic compensation mechanism. 536 *J. Geophys. Res.*.

Segev A., Michael Rybakov, Vladimir Lyakhovsky, Avraham Hofstetter, Gidon Tibor, Vladimir Goldshmidt, Zvi Ben Avraham., 2006. The structure, isostasy and gravity field of the Levant

continental margin and the southeast Mediterranean area, *Tectonophysics*, Volume 425, Issues 1-4, 13 Pages 137-157, DOI: 10.1016/j.tecto.2006.07.010.

Seitz, F. and M. Krugel. 2009. Inverse Model Approach for vertical Load Deformations in Consideration of Crustal Inhomogeneities. *In Geodetic Reference Frames*. P.23-29. DOI - 10.1007/978-3-642-00860-3\_4

Sengor, A. M. C. Natal in, B. A. 2001. Rifts of the world. SPECIAL PAPERS- GEOLOGICAL SOCIETY OF AMERICA ;pages 389-482

Sexton W.J. and Maylo Murday. 1994. The morphology and sediment character of the coastline of Nigeria: the Niger Delta. *Journal of Coastal Research*, Vol. 10, No. 4 ;pp. 959-977

Shunk A.J., Driese, S.G. and G. Michael Clark. 2006. Latest Miocene to earliest Pliocene sedimentation and climate record derived from paleosinkhole fill deposits, Gray Fossil Site, northeastern Tennessee, U.S.A., *Palaeogeography, Palaeoclimatology, Palaeoecology*, Volume 231, Issues 3-4, Pages 265-278, DOI: 10.1016/j.palaeo.2005.08.001.

Sigaev, N.A. 1959. Main tectonic Features of Egypt Republic. G.E. Organization for Geological Research and Mining Dept., Cairo, Egypt.

Simmons N. A., Forte, A.M., and S.P. Grand. 2007. Thermochemical structure and dynamics of the African superplume. *Geophysical Research Letters*; vol. 34, no.2

Simmons, N.A., Forte, A.M., Grand, S.P., 2009. Joint seismic, geodynamic and mineral physical constraints on three-dimensional mantle heterogeneity: Implications for the relative importance of thermal versus compositional heterogeneity, *Geophysical Journal International*, 177 (3), 1284-1304.

Simmons, N.A., Forte, A.M., Boschi, L., Grand, S.P. 2010. A Joint Tomographic Model of Mantle Density and Seismic Wave Speeds , *J. Geophys. Res.*, *in press*.

Sleep, N.H. 1971. Thermal effects of the formation of Atlantic continental margins by continental break-up. *Geophys. J.R. Astron. Soc.*, 24;p.325-350

Sloss, .L.L. 1963. Sequences in the cratonic interior of North America. *Geological Society of America Bulletin*, v. 74, p. 93-114

Small, E.E., and Anderson, R.S. 1998, Pleistocene relief production in Laramide mountain ranges, western United States: *Geology*, v. 26, p. 123–126, doi:10.1130/0091-7613

Spasojevic, S., Liu, L., Gurnis, M., Müller, R.D., 2008. The case for dynamic subsidence of the U.S. east coast since the Eocene. *Geophys. Res. Lett.* 35, 08305.

Summerfield, M. A., and N. J. Hulton (1994), Natural controls of fluvial denudation rates in major world drainage basins, *J. Geophys. Res.*, 99(B7), 13,871–13,883, doi:10.1029/94JB00715.

Sykes, T.J.S., 1996. A correction for sediment load upon the ocean floor: uniform versus varying sediment density estimations—implications isostatic correction *Mar. Geol.* 133, 35–49.

Syvitski and Milliman 2007. Geology, geography, and humans battle for dominance over the delivery of fluvial sediment to the coastal ocean. *The Journal of Geology*; volume 115, p. 1–19  
DOI: 10.1086/509246

Talbot, M.R. and Martin A.J. Williams. 2009. Cenozoic Evolution of the Nile Basin The Nile. H.J. Dumont (ed.), *The Nile: Origin, Environments, Limnology and Human Use*. Springer Science Monographiae Biologicae, 2009, Volume 89, II, 37-60, DOI: 10.1007/978-1-4020-9726-3\_3

Tapley, B. J., J. Ries, S. Bettadpur, D. Chambers, M. Cheng, F. Condi, B. Gunter, Z. 629 Kang, P. Nagel, R. Pastor, T. Pekker, S. Poole and F. Wang. 2005. GGM02 - Improved 630 gravity field model from GRACE, *J. Geodesy*, doi:10.1007/s00190-005-0480-z.

Tsoulis, D. 2004 Spherical harmonic analysis of the CRUST 2.0 global crustal model. *Journal of Geodesy*; Volume 78 , p. 7- 11 .DOI - 10.1007/s00190-003-0360-3

Turcotte, D.L., Schubert, G., 2001. *Geodynamics: Applications of Continuum Mechanics to Geological Problems*, 2nd Edition. Cambridge University Press, Cambridge, United Kingdom.

Ussami, N., Shiraiwa, S., and Dominguez, J.M.L., 1999, Basement reactivation in a sub-Andean foreland flexural bulge: The Pantanal wetland, SW Brazil: *Tectonics*, v. 18, p. 25–39, doi: 10.1029/1998TC900004.

Van Arsdale, R., McCallister, N., and B. Waldron. 2007. Upland Complex of the central Mississippi River valley: Its origin, denudation, and possible role in reactivation of the New Madrid seismic zone. *GSA Special Papers*; v. 425, p. 177-192, doi: 10.1130/2007.2425(13)

Vita-Finzi, C. 2001. Neotectonics at the Arabian plate margins, *Journal of Structural Geology*, Volume 23, Issues 2-3, Pages 521-530, DOI: 10.1016/S0191-8141(00)00117-6.

Vital, H. and Karl Stattegger. 2000. Major and trace elements of stream sediments from the lowermost Amazon River. *Chemical Geology*, Volume 168, Issues 1-2, July 2000, Pages 151-168, ISSN 0009-2541, DOI: 10.1016/S0009-2541(00)00191-1.

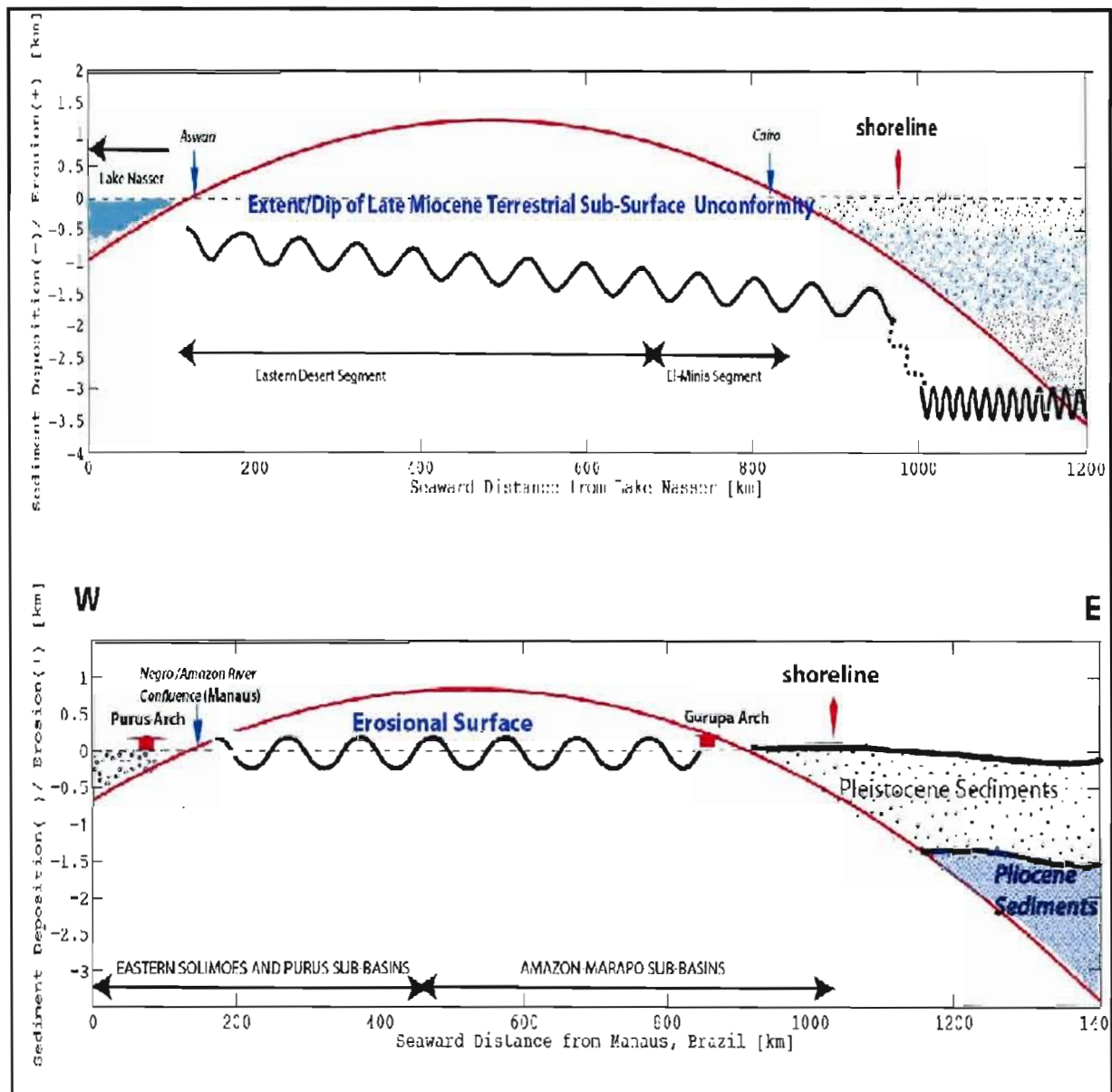
Von Blanckenburg, F. (2005), The control mechanisms of erosion and weathering at basin scale from cosmogenic nuclides in river sediment, *Earth Planet. Sci. Lett.*, 237, 462–479.

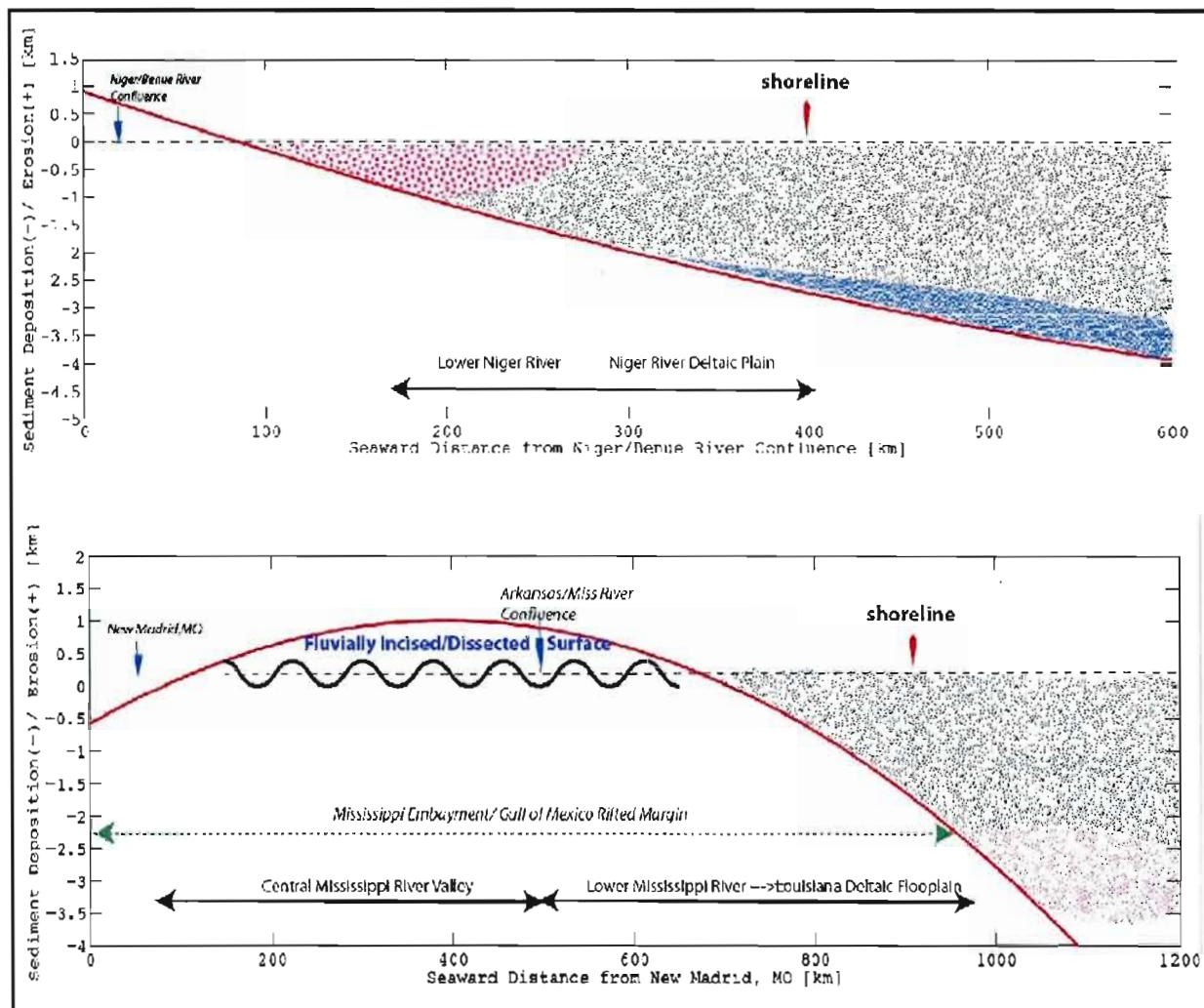
Watts, A., 2001. *Isostasy and Flexure of the Lithosphere*. Cambridge University Press, Cambridge, U.K. 458 pp.

Weimer, P. 1990. Sequence Stratigraphy, Facies Geometries, and Depositional History of the Mississippi Fan, Gulf of Mexico. *AAPG Bulletin*; Volume 74, Pages 425 - 453

- Wegmann, K.W., Brian D. Zurek, Christine A. Regalla, Dario Bilardello, Jennifer L. Wollenberg, Sarah E. Kopczynski, Joseph M. Ziemann, Shannon L. Haight, Jeremy D. Apgar, Cheng Zhao, and Frank J. Pazzaglia. 2007. Position of the Snake River watershed divide as an indicator of geodynamic processes in the greater Yellowstone region, western North America. *Geosphere*, 272 - 281.
- Wheeler, P., and N. White (2002), Measuring dynamic topography: An analysis of Southeast Asia, *Tectonics*, 21(5), 1040, doi:10.1029/2001TC900023
- Wheeler, P., and White, N., 2000, Quest for dynamic topography: Observations from Southeast Asia: *Geology*, v. 28p. 963-966 doi: 10.1130/0091-7613
- Whiteman, A. 1982. *Nigeria: its Petroleum Geology, Resources and Potential*, v.2. Graham and Trotman Ltd., 394 pp.
- Woodbury, H. O., Murray, Jr., I. B., Pickford, P. J. and W. H. Akers. 1973. Pliocene and Pleistocene Depocenters, Outer Continental Shelf, Louisiana and Texas. *AAPG Bulletin*, Volume 57, Issue 12 pp. 2428 - 2439
- Woodward, J.C., Macklin M.G., Krom, M. D. and MAJ Williams. 2007. The Nile: Evolution, quaternary river environments and material fluxes. In *Large Rivers: Geomorphology and Management* ed. Avijit Gupta, Ch.13 pp.261-292
- Wieczorek, M.A., 2007. Gravity and topography of the terrestrial planets. In: Spohn, T., Schubert, G. (Eds.), *Treatise on Geophysics*, vol. 10. Elsevier–Pergamon, Oxford, pp. 165–206.
- Zaki, R. 2007. Pleistocene evolution of the Nile Valley in northern Upper Egypt. *Quaternary Science Reviews*, Volume 26, Issues 22-24; pp.2883-2896, DOI: 10.1016/j.quascirev.2007.06.032.

Appendix 1: Schematic cross sections of imposed sedimentary loading/unloading along the longitudinal axes of Selected River/Fluvial Basins. See Chapter 4 Tables and Figures for reference. From Top to Bottom: Nile Basin, Amazon Basin, Mississippi Basin, Niger Basin.





AI cont'd

Appendix 2: Map view of transect paths superimposed on true earth topography (ETOPO2v2, top) and prescribed sedimentary loads and anti-loads (in meters, bottom)

